

# Segmentation of Underwater Multispectral Images with Applications in the Study of Coral Reefs

by

Francisco José Rivera Maldonado

A thesis submitted in partial fulfillment of the requirements for the degree of

MASTER OF SCIENCE

in


ELECTRICAL ENGINEERING

UNIVERSITY OF PUERTO RICO

MAYAGÜEZ CAMPUS

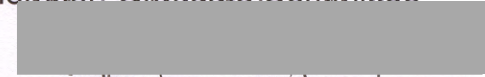
2004

Approved by:

  
Shawn D. Hunt, Ph.D.

Member, Graduate Committee

18 May 2004  
date

  
Miguel Vélez Reyes, Ph.D.


Member, Graduate Committee

17 de mayo de 2004  
date

  
Raúl E. Tores Muñiz, Ph.D.

President, Graduate Committee

18 de mayo de 2004  
date

  
Roy A. Armstrong, Ph. D.

Representative of Graduate Studies

17 de mayo de 2004  
date

  
Jorge L. Ortiz Álvarez

Chairperson of the Department

May 18, 2004  
date

## **Abstract**

The monitoring and studying corals reefs can be used to measure the effects of contamination in the ocean. An essential preliminary step for recognizing and analyzing corals reefs in an image is image segmentation. The main goal of image segmentation is to divide an image into parts that have a strong correlation with objects or areas of the real world contained in the image.

The segmentation algorithms used in this work can be divided in two areas: boundary detection – segmentation only across contour boundaries created by the objects and homogeneity analysis – segmentation across the quantification of the homogenous regions created by the objects. Two new algorithms based on these two areas were developed: new Hough transform for boundary detection algorithm (NHTBDA) and Hurst coefficient/Hough transform algorithm (HCHTA). The developed algorithms were compared with other two homogeneity based algorithms presented in the literature. The performance of the algorithms and the results of the segmentation are tested and analyzed in: underwater multispectral images generated in a controlled environment, underwater multispectral images taken by an Autonomous Underwater vehicle (AUV), and remotely sensed images.

## Resumen

El monitoreo y el estudio de los arrecifes de corales se puede utilizar para medir los efectos de la contaminación en el océano. Un paso preliminar esencial para reconocer y analizar los arrecifes de corales en una imagen es segmentación de la imagen. La meta principal de la segmentación de la imagen es dividir una imagen en partes que tienen una alta correlación con los objetos o las áreas del mundo verdadero contenido en la imagen.

Los algoritmos de segmentación utilizados en este trabajo se pueden dividir en dos áreas: detección de fronteras – segmentación a través de los límites del contorno creados por los objetos y análisis de homogeneidad – segmentación a través de la cuantificación de las regiones homogéneas creadas por los objetos. Dos nuevos algoritmos basados en estas dos áreas fueron desarrollados: algoritmo de la nueva transformada de Hough para la detección de fronteras (NHTBDA) y el algoritmo del coeficiente Hurst/transformada Hough (HCHTA). Los algoritmos desarrollados fueron comparados con otros dos algoritmos basados en la homogeneidad presentados en la literatura. El funcionamiento de los algoritmos y los resultados de la segmentación se comprueban y se analizan en: imágenes multiespectrales generadas en ambiente controlado, imágenes multiespectrales subacuáticas tomadas por un vehículo subacuático autónomo (AUV), e imágenes detectadas remotamente.

## **Dedictory**

*To my family for sharing with me all my achievements and unconditional support.*

*To Zaida Iris for always believing in me.*

## Acknowledgments

I want to thank my advisor, Dr. Raúl Torres for his guidance, dedication, and faith in me made a difference in my work and my life. Thanks to my member of my graduate committee, Dr. Miguel Velez, Dr. Shawn Hunt, Dr. Hamed Parsiani, and Dr. Roy Armstrong for helping me in this work.

Thank to the collaboration of Juan Torres for the classification of the AUV images and Dr. Hanumant Singh from Wood Hole Oceanographic Institute and Dr. Roy Armstrong from the Department of Marine Science of the University of Puerto Rico at Mayagüez for the digital coral images obtained using the SeaBED AUV.

Thanks to all the personnel of LARSIP and CenSSIS: Rosa, Marie, Vanessa, Maribel, and Claribel and specially Emmanuel Arzuaga. Special thanks to all the people in the laboratory for all the good times, friendship, and help.

**This work was supported in part by CenSSIS, the Center for Subsurface Sensing and Imaging Systems, under the Engineering Research Centers Program of the National Science Foundation (Award Number EEC-9986821).**

## TABLE OF CONTENT

<b>Abstract .....</b>	<b>ii</b>
<b>Resumen.....</b>	<b>iii</b>
<b>Dedicatory.....</b>	<b>iv</b>
<b>Acknowledgments.....</b>	<b>v</b>
<b>TABLE OF CONTENT .....</b>	<b>vi</b>
<b>LIST OF TABLES.....</b>	<b>viii</b>
<b>LIST OF FIGURES .....</b>	<b>ix</b>
<b>Chapter 1: Introduction.....</b>	<b>1</b>
1.1 What is image segmentation? .....	1
1.2 Developed algorithms .....	2
1.3 Justification.....	2
1.4 Objectives.....	4
1.5 Chapters Overview .....	5
<b>Chapter 2: Literature Review .....</b>	<b>6</b>
2.1 Basic digital image processing and multispectral imagery.....	6
2.1.1 What is a digital image? .....	6
2.1.2 Multispectral imagery.....	7
2.2 Image segmentation on multispectral images .....	9
2.3 Boundary detection .....	10
2.3.1 Hough transform .....	10
2.3.1.1 Slope-intercept Hough transform .....	11
2.3.1.2 Parameterized Hough transform .....	12
2.3.1.3 Advantages and disadvantages of the Hough transform .....	14
2.3.1.4 Relevant publications .....	15
2.4 Homogeneity analysis .....	17
2.4.1 Local homogeneity coefficient .....	17
2.4.2 Hurst coefficient .....	19
2.4.3 Peer group coefficient .....	23
<b>Chapter 3: Procedure.....</b>	<b>26</b>
3.1 New Hough transform for boundary detection algorithm (NHTBDA) .....	26
3.1.1 First stage-image pre-processing and Hough transform.....	27
3.1.1.1 Image enhancement .....	27
3.1.1.2 Edge Detector .....	28
3.1.1.3 Hough transform .....	29

3.1.2	Second stage – Clustering .....	29
3.1.2.1	Fuzzy c-means algorithm .....	30
3.1.3	Third stage – False contours elimination .....	31
3.2	Local homogeneity analysis algorithm (LHAA) .....	32
3.2.1	Image pre-processing .....	33
3.2.2	Spatial Segmentation .....	33
3.2.2.1	Local homogeneity coefficient .....	33
3.2.2.2	Seeded Region growing .....	34
3.2.2.3	Region merging .....	35
3.3	Hurst coefficient / Hough transform algorithm (HCHTA) .....	35
3.3.1	Hurst coefficient using the Hough transform .....	36
3.3.2	Weighted c-means .....	37
3.3.3	Spatial Segmentation .....	38
3.4	Perceptual image quantization algorithm (PIQA) .....	39
3.4.1	Peer group coefficient .....	39
3.4.2	Weighted c-means .....	40
3.4.3	Spatial segmentation .....	40
<b>Chapter 4: Results</b>	.....	<b>41</b>
4.1	Underwater multispectral images generated in a controlled environment	41
4.1.1	First image: pencil .....	41
4.1.2	Second image: nut .....	44
4.1.3	Third image: tank bottom with objects .....	46
4.2	Underwater multispectral image taken by an Autonomous Underwater Vehicle (AUV) .....	50
4.3	Remotely sensed underwater multispectral image .....	61
4.4	Summary and discussion of results .....	65
<b>Chapter 5: Conclusion</b>	.....	<b>68</b>
5.1	Summary .....	68
5.2	Conclusions .....	69
5.3	Future work .....	71
<b>References</b>	.....	<b>72</b>

## LIST OF TABLES

Table 2.1 Distance of pixels from the central pixel.....	21
Table 4.1 Details of the first multispectral underwater image generated in a controlled environment: pencil.....	42
Table 4.2 Details of the second multispectral underwater image generated in a controlled environment: nut.....	44
Table 4.3 Details of the third multispectral underwater image generated in a controlled environment: tank bottom with objects.....	46
Table 4.4 Details of the underwater multispectral image taken by an AUV.....	50
Table 4.5 Composition of classes of each image of Figure 4.10 .....	58
Table 4.6 Classification results of Figure 4.10a .....	58
Table 4.7 Classification results of Figure 4.10b .....	59
Table 4.8 Classification results of Figure 4.10c .....	59
Table 4.9 Classification results of Figure 4.10d.....	59
Table 4.10 Details of the remotely sensed underwater multispectral image taken by IKONOS .....	61



## LIST OF FIGURES

Figure 2.1 Image representation: (a) axis convention and (b) digital image 3x3 pixel array representation. ....	7
Figure 2.2 Multispectral image with pixel visualization. Images are taken simultaneously at different wavelength. ....	8
Figure 2.3 Slope-intercept Hough transform: (a) Image space and (b) Hough parameter space. ....	12
Figure 2.3 Parameterized Hough transform: (a) Image space and (b) Hough parameter space. ....	13
Figure 2.4 Example using the parameterized Hough transform on noisy image: (a) Original noisy image, (b) Hough transform parameter space, and (c) lines detected in the original image. ....	14
Figure 2.6 Example of different patterns and their correspondent LHC values ..	19
Figure 2.7 Circular 7-pixel neighborhood used for Hurst coefficient calculation	21
Figure 2.8 Straight line fit to the log(Distance) vs. log(Range) for a 7 pixel wide circular window. The slope is the Hurst coefficient. ....	22
Figure 3.1 Segmentation using the Hough transform for boundary detection.....	27
Figure 3.2 Underwater multispectral image of a pencil example: (a) one band of the multispectral pencil image and (b) results after noise removal and histogram equalization of image 3.2a. ....	28
Figure 3.3 Sobel edge detector example result on the enhance image in figure 3.2a .....	28
Figure 3.4 Hough transform of the multispectral pencil image: (a) Hough space and (b) Hough transform detected lines.....	29
Figure 3.5 Fuzzy c-means results for the multispectral pencil image using two clusters .....	31
Figure 3.6 Segmentation using local homogeneity analysis algorithm. ....	32
Figure 3.7 H-image for the underwater multispectral image of a pencil using a 3x3 square window. ....	33
Figure 3.8 Over segmented seeded region growing of the underwater multispectral image of a pencil. ....	35
Figure 3.9 Segmentation using Hurst coefficient / Hough transform algorithm..	36
Figure 3.10 Hurst coefficient using the Hough transform image of a pencil using 7x7 circular window. ....	37
Figure 3.11 Weighted image of Hurst coefficient using the Hough transform of a pencil using a 7x7 circular window.....	37

Figure 3.12 Segmentation using the perceptual image quantization algorithm...	39
Figure 3.13 Peer group coefficient image of a pencil using a 3x3 square window. .....	39
Figure 3.14 Weighted image of peer group coefficient of a pencil using a 3x3 square window. ....	40
Figure 4.1 First underwater multispectral image generated in a controlled environment: pencil. ....	42
Figure 4.2 Segmentation results of the first image using: (a) new Hough transform for boundary detection, (b) local homogeneity analysis, (c) Hurst coefficient / Hough transform, and (d) perceptual image quantization. ....	43
Figure 4.3 Second underwater multispectral image generated in a controlled environment: nut. ....	44
Figure 4.4 Segmentation results of the second image using: (a) new Hough transform for boundary detection, (b) local homogeneity analysis, (c) Hurst coefficient / Hough transform, and (d) perceptual image quantization. ....	45
Figure 4.5 Third underwater multispectral image generated in a controlled environment RGB visualization: tank bottom with objects. ....	47
Figure 4.6 Segmentation results of the second synthetic image using: (a) new Hough transform for boundary detection, (b) local homogeneity analysis, (c) Hurst coefficient / Hough transform, and (d) perceptual image quantization. ....	49
Figure 4.7 Two underwater multispectral RGB images taken by an AUV .....	51
Figure 4.8 Classification map of the underwater multispectral image taken by an AUV using Canvas 8.0.3 <sup>1</sup> .....	52
Figure 4.9a Segmentation results of both AUV image using local homogeneity analysis. ....	53
Figure 4.9b Segmentation results of both AUV image using Hurst coefficient / Hough transform .....	54
Figure 4.9c Segmentation results of both AUV image using perceptual image quantization. ....	55
Figure 4.10 Set of AUV images with class maps done in Canvas In the class maps, the corals regions are in white and background regions are in black. ....	57
Figure 4.11 Region growing result of Hurst coefficient/Hough transform with 451 regions.....	60
Figure 4.12 Classification of the corals using the supervised merging algorithm on the region growing result of Hurst coefficient/Hough transform.....	61
Figure 4.13 RGB visualization of IKONOS image of La Parguera, Enrique Reef denoted. ....	62
Figure 4.14 RGB visualization of IKONOS image of Enrique reef area .....	62

Figure 4.15 Classification map of Enrique Reef in 1980 [40].....	63
Figure 4.16 Segmentation results of Enrique Reef using local homogeneity analysis. ....	63
Figure 4.17 Segmentation results of Enrique Reef using: (a) Hurst coefficient / Hough transform and (b) perceptual image quantization. ....	64

## **Chapter 1: Introduction**

### **Preview**

The Center for Subsurface Sensing and Imaging Systems (CenSSIS) is a center for the advancement of subsurface sensing and imaging studies. The main purpose of CenSSIS is to study how to detect and create images of objects and conditions underground, underwater, or embedded within living tissue or manmade structures. Many different researches in the area of image processing are carried by this engineering research center. One important tool in image processing that is investigated in CenSSIS is image segmentation.

### **1.1 What is image segmentation?**

Image segmentation is an essential preliminary step in most automatic pictorial pattern recognition and scene analysis problems, and is one of the most frequent and necessary tasks in the area of computer vision. The main goal of image segmentation is to divide an image into parts that have a strong correlation with objects or areas of the real world contained in the image. Image segmentation consists of dividing an image into regions that represents objects that either have some measure of homogeneity within them, or have some measure of contrast with the objects or their edges. Most image segmentation algorithms are modifications, extension, or combinations of these two basic concepts—homogeneity and contrast. The level to which these concepts are divided depends on the problem being solved.

## **1.2 Developed algorithms**

Many different algorithms have been developed to achieve image segmentation over the years. The choice of one segmentation algorithm over another is dictated mostly by the peculiar characteristic of the problem being considered. The problem is to decide which segmentation algorithms are well suited in performing segmentation to objects in underwater multispectral images and applying the algorithms to the images. The particular interest is in underwater images containing a desired object of varying size and shape, which can be partially covered by a medium. The objects of interest in the underwater image are the corals and corals reefs.

The image segmentation algorithms proposed in this work are based in the fusion of the widely used Hough transform (HT) and clustering segmentation techniques and maintaining in consideration the homogeneity of the objects in the images. The estimation of parameters using the HT is used as an essential part of the two algorithms developed: new HT for boundary detection and HT for homogeneity analysis.

## **1.3 Justification**

The advantage of using the Hough transform over other segmentation algorithms is that it can estimate the different parameters needed, even under low contrast and noisy images usually present in underwater images.

Preliminary work has shown that the HT is an efficient tool for the estimation of parameters in noisy and contaminated data [1]. In CenSSIS, because the data (images) of interest are of subsurface objects, this noise and contamination exists.

The first algorithm, HT for boundary detection achieves segmentation only across contour boundaries created by the objects in the image [2]. In this context, the HT is a tool created to estimate lines in these boundaries, and later expanded to determine the real geometric shape of objects. The HT for boundary detection has several known challenges such as the end point (infinite lines) and connectivity problem which lead to false contours estimation. The algorithm introduces a new approach to eliminate false contours from the extrapolation of lines in the Hough Transform. The algorithms use clustering segmentation information in the original image to capture the local properties of the desired object. The boundary information (HT) and local properties (clustering) of the desired object are fused together and false contours are eliminated.

The second algorithm, homogeneity analysis using the HT achieves segmentation across contour boundaries created by the objects themselves and the spatial homogeneity in the image. The HT estimates the parameters of homogeneity in the image. The HT for homogeneity analysis has several known challenges such as the over segmentation problem. The algorithm introduces an approach based on the variance of the data to estimate the quantization levels for the HT accumulator space and cluster merging techniques for the over segmentation problem.

The algorithms developed in this research are compared in terms of the performance against other existent algorithms. All algorithms are performed in remotely sensed images; underwater multispectral images generated in a controlled environment containing known objects of varying size and shape; and underwater multispectral images taken by an Autonomous Underwater Vehicle (AUV).

## **1.4 Objectives**

The main objective of this work was to develop a segmentation algorithm with application in the study of coral reefs considering the spatial information of the objects of interest in the image.

The specific objectives of this work were:

- Understand the concepts of image segmentation based on the Hough transform and homogeneity analysis.
- Develop a segmentation algorithm based on the fusion of the Hough transform with clustering segmentation techniques to perform segmentation in underwater multispectral images containing desired objects of varying sizes and shapes that can be partially covered by different mediums.
- Elimination of false contours from the extrapolation of lines in the Hough Transform.

- Develop a segmentation algorithm based on homogeneity analysis and the Hough transform to perform segmentation in underwater multispectral images containing desired objects of varying sizes and shapes that can be partially covered by different mediums.
- Test and analyze the performance and the results of the segmentation algorithms in remotely sensed images; underwater multispectral images generated in a controlled environment containing known objects of varying size and shape; and underwater multispectral images taken by an Autonomous Underwater Vehicle (AUV).

## **1.5 Chapters Overview**

Chapter 2 presents a literature review for the theory utilized in this research. Basic image processing theory will be presented as well as the Hough transform for parameter estimation, homogeneity analysis measurement, etc. Chapter 3 presents the algorithms that have been developed and used: Hough transform for boundary detection, local homogeneity analysis, Hurst coefficient/Hough transform for homogeneity analysis, and peer image quantization. Chapter 4 presents the results of the algorithms developed and a comparison in terms of the performance against all the algorithms discussed. Chapter 5 consists of a summary, achievements and conclusions concerning this thesis and recommendations for further work.



## Chapter 2: Literature Review

### Preview

In this chapter, a literature review for the theory utilized in this research is presented and divided in four parts. The first part of the chapter introduces the basics of image processing and multispectral imaging. The second part introduces basic concepts of multispectral segmentation. The third part introduces the boundary detection algorithms that are more relevant to this work like the Hough transform. The fourth part introduces the methods that measure the local homogeneity using overlapping windows that are more relevant to this work like the local homogeneity coefficient, the peer group coefficient, and the Hurst coefficient.

## 2.1 Basic digital image processing and multispectral imagery

### 2.1.1 What is a digital image?

A monochrome image or image (**figure 2.1a**) refers to a two dimensional light intensity function  $f(x, y)$ , where  $x$  and  $y$  denote spatial coordinates and the value of  $f$  at any point  $x$  and  $y$  is proportional to the brightness (or gray levels) of the image at that point [3].

A digital image (**figure 2.1b**) is an image that has been discretized both in spatial coordinates and brightness. A digital image can be considered as a matrix

whose row and column indices identify the gray level at that point. The elements of such a digital array are called picture elements or pixels. A number represents each pixel.

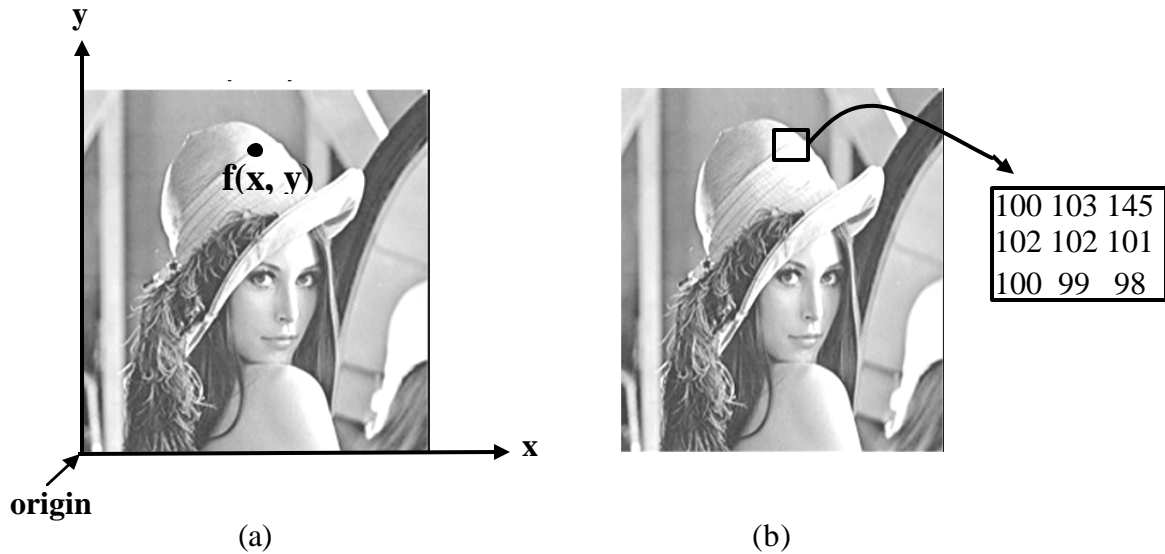


Figure 2.1 Image representation: (a) axis convention and (b) digital image 3x3 pixel array representation.

### 2.1.2 Multispectral imagery

A multispectral image is an image that is acquired at different wavelengths [4]. Multispectral image can be seen as the gray levels of the image at each wavelength (**figure 2.2**). The different wavelength images in multispectral images are called spectral bands.

Multispectral sensors acquire data in a few number spectral bands of the electromagnetic spectrum. The spectral resolution or spectral difference between bands in multispectral images is lower in comparison with what is called hyperspectral images. Remember that a number represents each pixel in

monochromatic images. In a multispectral image, a vector of numbers represents each pixel.

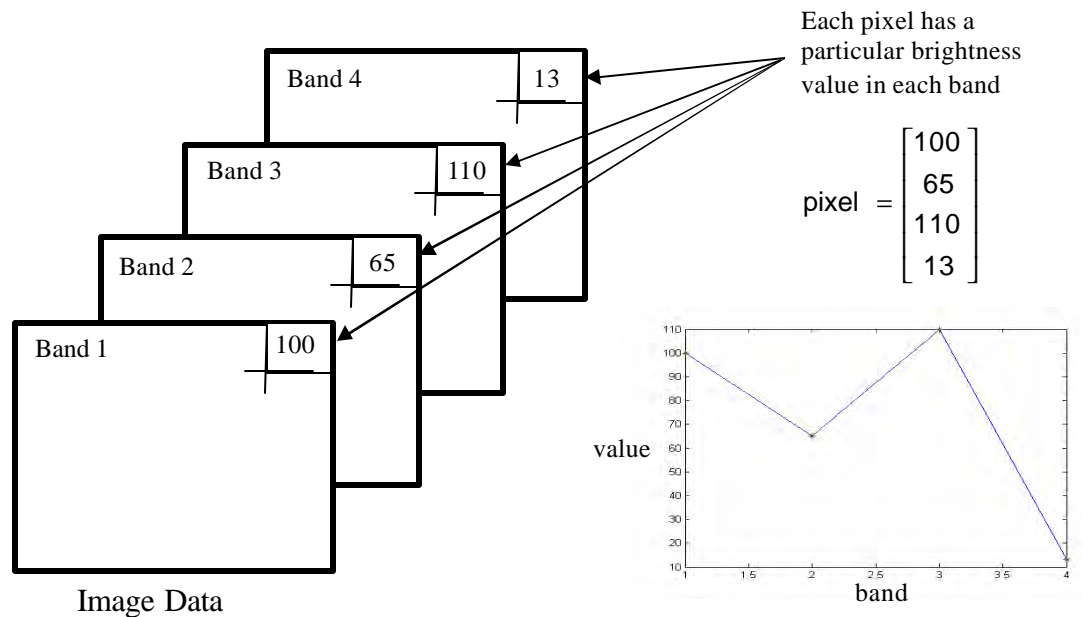


Figure 2.2 Multispectral image with pixel visualization. Images are taken simultaneously at different wavelength.

The spectral information can be very helpful in the segmentation of multispectral images since it is known that a certain object has distinctive spectral information. This distinctive spectral information or spectral signature of the object can be used to discriminate between other objects in the image since other objects have different spectral signatures. Spectral signature can be seen somehow as a fingerprint of a person; it can be differentiable from another person.

## 2.2 Image segmentation on multispectral images

The particular interest for the segmentation is in underwater multispectral images containing corals and corals reefs. Low contrast and noise usually is present in underwater images. Segmentation algorithms for multispectral images generally are based on one of two basic concepts: contrast and homogeneity of the objects or regions contained in the image. An algorithm that takes in account these two basic concepts is needed.

In the first concept, the approach is to partition an image based on abrupt changes in pixel value [3]. The principal areas of interest within this category are detection of isolated points and detection of lines and edges in an image. Several techniques like edge detectors yield pixels lying only on the boundary between objects or regions. This set of pixels rarely characterized a boundary completely because of noise, breaks in the boundary from non-uniform illumination, and other effects that introduce spurious intensity discontinuities. Typically, edge detection algorithms are followed by a boundary detection procedure designed to assemble edge pixels into meaningful boundaries.

In the concept of homogeneity, the approach for image segmentation is to partition an image based on a quantitative similarity of the pixels [3]. Some of the criteria for homogeneity are: texture, shape, model, spectral signature, color, and gray-level. The principal areas of interest within this category are the detection of similar regions of pixels in an image based on texture analysis, clustering, spectral signature similarity, region growing and region splitting and merging. Partitioning an image in regions based on a quantitative similarity or

homogeneity of the pixels is generally better in noisy images where edges are extremely difficult to detect.

## **2.3 Boundary detection**

The main goal of boundary detection is to reconstruct edge pixels into meaningful boundaries. Many algorithms exist for boundary detection. The Hough transform is a powerful boundary detection procedure. The advantage of using the Hough transform is that it can estimate the boundary of the objects or regions needed, even under low contrast and noisy images usually present in underwater images. The Hough transform has been widely used in monochromatic images and the fact that it can cope with noise is desired in developing an algorithm. A version of the Hough transform can be modified for multispectral images

### **2.3.1 Hough transform**

The Hough transform for line estimation was first introduced by Paul Hough [5] in 1962 to detect straight lines in a bubble chamber data. Since the introduction in 1962, the HT has long been recognized in many articles as a robust technique for the detection of analytically defined shapes in an image as it can handle partially occluded and noise corrupted conditions. The abundant literature about the Hough Transform for line and shape recognition can be classified into two groups depending on the parameterization used for

expressing the lines [6]: the slope-intercept Hough transform and the parameterized Hough transform. However, an aspect that is common to all the algorithms developed is that they require the application of an edge detector to the image before starting with the recognition process because binary images are needed.

### 2.3.1.1 Slope-intercept Hough transform

The slope-intercept Hough transform uses the parameters  $m$  and  $c$  to express the lines, where  $m$  is the slope and  $c$  is the point of intersection with the ordinate axis. Each boundary point  $(x_i, y_i)$  of an image space generates a straight line in a parameter space according to the equation

$$c_i = -x_i * m + y_i \quad (2.1)$$

where  $x_i$  play the role of the slope, and  $y_i$  takes the value of the point of intersection with the ordinate axis [7]. This means that any straight line in the image is represented by a single point in the  $m$ - $c$  parameter space and any part of this straight line is transformed into the same point. The main idea of the line detection is to determine all the possible line pixels in the image, to transform all lines that can go through these pixels into corresponding points in the parameter space, and to detect the points  $(m, c)$  in the parameter space that frequently resulted from the Hough transform of lines  $y = m * x + c$  in the image [8]. **Figure 2.3** illustrates this concept.

Some different techniques of the slope-intercept Hough transform are the binary Hough transform (BHT) [9, 10], the randomized Hough transform (RHT) [11, 12, 13], and the fast Hough transform (FHT) [14]. Note that a problem using

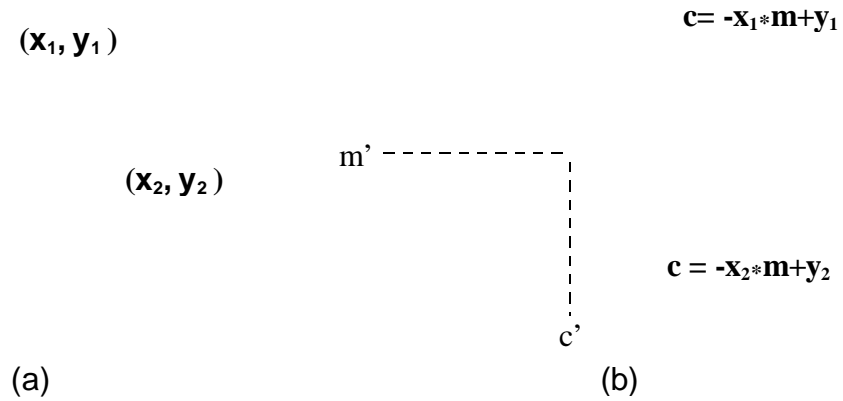


Figure 2.3 Slope-intercept Hough transform: (a) Image space and (b) Hough parameter space.

the equation  $y = m * x + c$  to represent a line is that both the slope and the intercept approaches infinity as the line approach the vertical (infinite slopes). Another form of the Hough transform is needed.

### 2.3.1.2 Parameterized Hough transform

The second and most abundant group corresponds to those using the parameters  $\rho$  and  $\theta$ . This parameterized version of the HT [15], states that if a line whose normal makes an angle  $\theta$  with the  $x$  axis, and has distance  $\rho$  from the origin is considered, the equation of the line corresponding to any point  $(x_i, y_i)$  on this line is given by the formula

$$\rho = x_i \cos(\theta) + y_i \sin(\theta) \quad (2.2)$$

In an image analysis context, the coordinates of the point(s) of edge segments (*i.e.*  $(x_i, y_i)$ ) in the image are known and therefore serve as constants in the parametric line equation, while  $\rho$  and  $\theta$  are the unknown variables we seek.

The possible  $(\rho, \theta)$  values defined by each pixel  $(x, y)$ , points in Cartesian image space map are plotted to curves (*i.e.* sinusoids) in the polar Hough parameter space. This point-to-curve transformation is the Hough transformation for straight lines. When viewed in Hough parameter space, points which are collinear in the Cartesian image space become readily apparent as they yield curves which intersect at a common  $(\rho, \theta)$  point. The transform is implemented by quantizing the Hough parameter space into finite intervals or accumulator cells. As the algorithm runs, each  $(x_i, y_i)$  is transformed into a discretized  $(\rho, \theta)$  curve and the accumulator cells which lie along this curve are incremented. Resulting peaks in the accumulator array represent strong evidence that a corresponding straight line exists in the image. **Figure 2.4** illustrates this concept.

The  $(\rho, \theta)$  form has become the most familiar parameterization method of the line detection in using the Hough transform, and the associated transform is termed the standard Hough transform (SHT) [16]. The Hough transform is widely used in many applications where boundary description of a desired

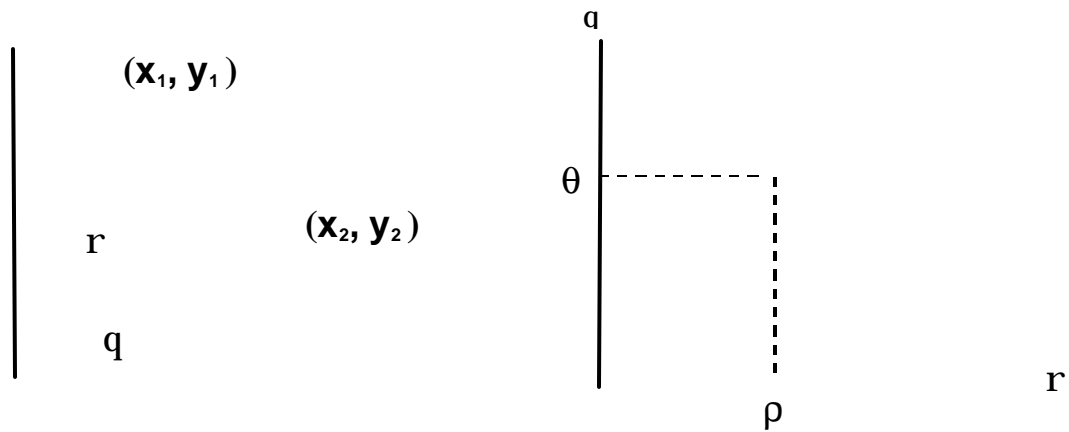


Figure 2.3 Parameterized Hough transform: (a) Image space and (b) Hough parameter space.



object is needed in an image. It has been recognized as a robust technique as it can handle partially occluded and noise corrupted conditions of the object in the image; but, also has several known challenges such as the end point (infinite lines) and connectivity problem which lead to false contours.

### 2.3.1.3 Advantages and disadvantages of the Hough transform

The advantage of using the Hough transform over other boundary detection algorithms is that it can detect lines on corrupted and noisy images (**figure 2.5**). Each edge-detected pixel contributes to the global solution, so collinear pixels contribute in the finding of lines in the image.

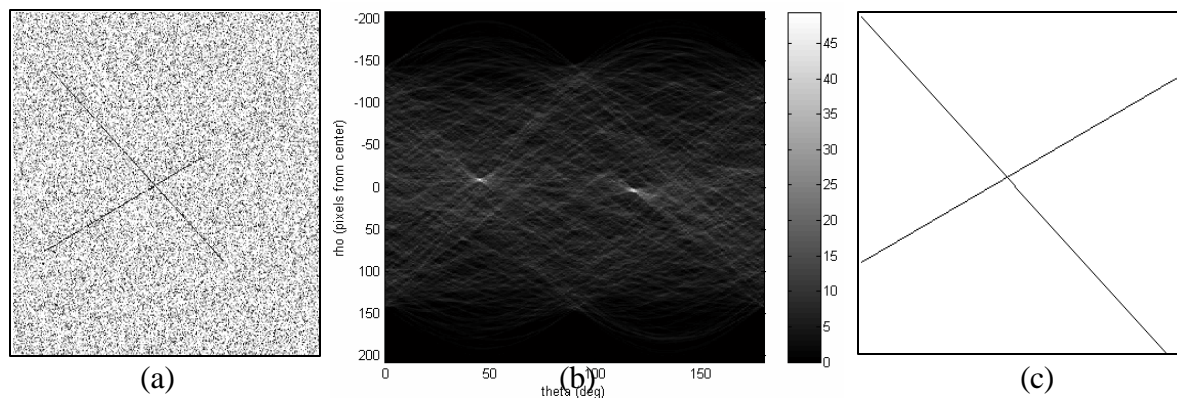


Figure 2.4 Example using the parameterized Hough transform on noisy image: (a) Original noisy image, (b) Hough transform parameter space, and (c) lines detected in the original image.

As stated before, the slope-intercept Hough transform has the problem that the slope approaches infinity as the line approaches the vertical (infinite slopes). So, the slope-intercept Hough transform cannot be used because vertical lines in the image space cannot be detected. One way around this problem is to use the parameterized representation of the Hough transform. The

parameterized version has several known challenges due to the fact that only the different  $(\rho_n, \theta_n)$  are known in the parameter space [16]:

1. Connectivity problem –the HT accumulator array add each point in the image that have the same parameters. These points may belong to different parts of the image.
2. End points problem – results from the accumulator can only provide the equations of the detected lines, instead of line segments with finite length.

#### **2.3.1.4 Relevant publications**

Some of the most relevant publications related with the usage of the Hough transform are described below.

Hanif *et al.* [17] addresses the problems from the computation of the standard Hough transform such as: the connectivity problem and the end point problem. A new algorithm for the detection of endpoints is presented. The algorithm cannot detect the intersecting point between two perpendicular lines.

Princen *et al.* [18] and Hare *et al.* [19] present a thorough study between different Hough transform algorithms: the standard HT, the adaptive HT, the fast HT and the hierarchical HT (Princen *et al.*) and the randomized HT, the counter-based HT, and the fast incremental HT (Hare *et al.*). The result of the study indicates that the standard HT gives more accurate results for line detection but its computational expensive.

J. Vuillemin [20] and Aggarwal *et al.* [21] presents the usage of the Radon transform to compute the Hough transform. The Hough transform and the Radon transform are identical if some of the sampling parameters are restricted. The Radon transform offers another way for the computation of the Hough transform.

Raymond K.K. Yip [16] presents a modified SHT for line segment extractions named line patterns Hough transform (LPHT). Using the concept of relative connectivity of points on a line segment is voted in a 2-dimensional accumulator, which has the same resolution as the image.

Tezmol *et al.* [22] addresses the issues involved in developing a robust segmentation technique capable of finding the location and orientation of the cervical vertebrae in x-ray images. A customized approach, based on the SHT, captures shape variability to overcome noise and occlusions. The approach effectively finds an estimation of the locations of the cervical vertebrae boundaries in digitalized x-rays.

Yalin *et al.* [23] presents the usage of a modified standard Hough transform in lumbar vertebrae segmentation. The usage of genetic algorithms is combined with the SHT to search the accumulator Hough space and false peak was avoided.

Han *et al.* [24] and Soodamani *et al.* [25] present the usage of fuzzy logic techniques in the computation of a modified Hough transform for shape

detection in images. Fuzzy Hough transform improves the segmentation results in images.

## **2.4 Homogeneity analysis**

The main goal in homogeneity analysis algorithms is to decompose an image to textually homogeneous regions. Texture can be seen as one of the main difficulties facing a segmentation method. For the images that contain only homogeneous spectral regions, many existing segmentation techniques, such as clustering can work well. Unfortunately, subsurface images are rich in both spectral variability and texture. Most of the texture segmentation algorithms require the estimation of texture model parameters, which is a hard problem and often based on good homogeneous regions.

Three different methods that quantify the local homogeneity in the image using overlapping windows at different scales are used to efficiently handle texture. Using the overlapping windows, each pixel in the image is compared with its window neighbors to calculate a coefficient that measure the homogeneity. The three methods used are: local homogeneity coefficient, Hurst coefficient, and peer group coefficient.

### **2.4.1 Local homogeneity coefficient**

Local homogeneity coefficient (LHC) is applied on a local overlapping window in the image to measure the homogeneity of a pattern. LHC was first

introduced by Jing *et al.* [26] in 2003 for the unsupervised segmentation of color images considering texture.

Let  $(x, y)$  denote the location of a pixel in the image and  $l(x, y, z)$  the spectral response of pixel  $(x, y)$  at band  $z = 1, 2, \dots, M$ . Let  $P$  be the pattern to compute homogeneity. Consider  $P$  to be an overlapping window that can be of any symmetric shape. The most used windows are the squared and circular windows. Let  $(x_c, y_c)$  be the center of the pattern with the spectral response being  $l(x_c, y_c, z)$ . Each pixel  $p_i = (x_i, y_i)$  in  $P$  corresponds to a vector  $c_{p_i} = (x_i - x_c, y_i - y_c)$  where  $i=1, 2, \dots, k = \text{\#pixels in window}$ . Based on  $c_{p_i}$ , a new vector is constructed

$$f_i(z) = (l(x_i, y_i, z) - l(x_c, y_c, z)) \cdot \frac{[(x_i - x_c), (y_i - y_c)]}{\|[(x_i - x_c), (y_i - y_c)]\|_2} \quad (2.3)$$

Now, let  $f$  be the sum of all vectors defined in  $P$

$$f(z) = \sum_{i=1}^k f_i(z) \quad (2.4)$$

The homogeneity value is given by

$$H(z) = \|f(z)\|_2 \quad (2.5)$$

Now,

$$H = \begin{bmatrix} H(1) \\ H(2) \\ \vdots \\ H(M) \end{bmatrix} \quad (2.6)$$

Finally, the local homogeneity coefficient (LHC) is given by

$$\text{LHC} = \|H\|_2 \quad (2.7)$$

As an example in **Figure 2.6**, assume the value of ' $*$ ' < value of ' $\mathbf{x}$ ' and a 3x3 squared window.

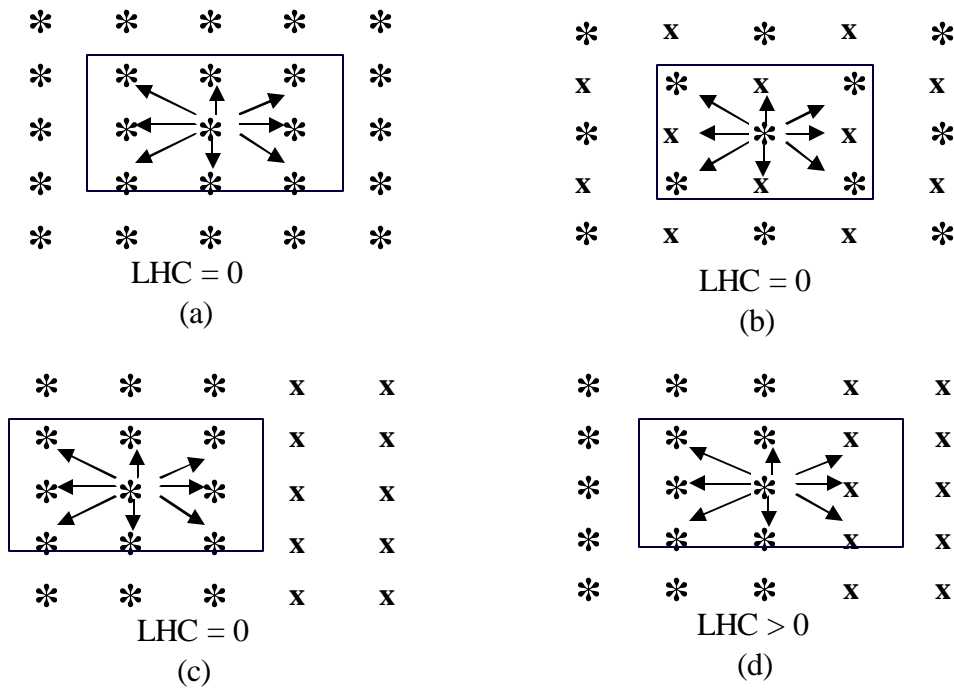


Figure 2.6 Example of different patterns and their correspondent LHC values

From the previous figure, we can see that the LHC is lower if the central pixel is near a homogeneous region (**Figures 2.6a, 2.6b, 2.6c**) and the LHC is higher if the central pixel is near a region boundary (**Figure 2.6d**).

#### 2.4.2 Hurst coefficient

Fractal geometry can be used to compute the homogeneity between groups and discriminate between textures. Fractal refers to entities (especially sets of pixels) that display a degree of self-similarity at different scales [27]. The characterization of surfaces from elevation images by a fractal dimension.

The fractal dimension  $D$  of a set of pixels  $I$  is specified by the relationship

$$1 = Nr^D \quad (2.8)$$

where the image  $I$  has been broken up into  $N$  non-overlapping copies of a basic shape, each one scaled by a factor of  $r$  from the original. A particularly efficient method for computing the fractal dimension  $D$  of surfaces from elevation images is the Hurst coefficient, or rescaled range analysis [28, 29, 30]. The equation 2.4 can be rewritten as

$$D = \frac{\log(N)}{\log\left(\frac{1}{r}\right)} \quad (2.9)$$

From this equation, it can be seen that there is a log-log relationship between  $N$  and  $r$ . If  $\log(N)$  were plotted against  $\log(r)$  the result should be a straight line whose slope is approximately  $D$ . The Hurst coefficient is an approximation that makes use of this relationship.

Overlapping symmetric windows are used to calculate the Hurst coefficient. Circular windows are the most used windows for the computation of the Hurst coefficient. **Figure 2.6** shows a neighborhood region consisting of 37 pixels in a 7-pixel wide circular shape. Eight regions are marked according to the distance of each pixel from the central pixel, see **Table 2.1**. Within each group, the largest difference (or the range) in gray-level is found.





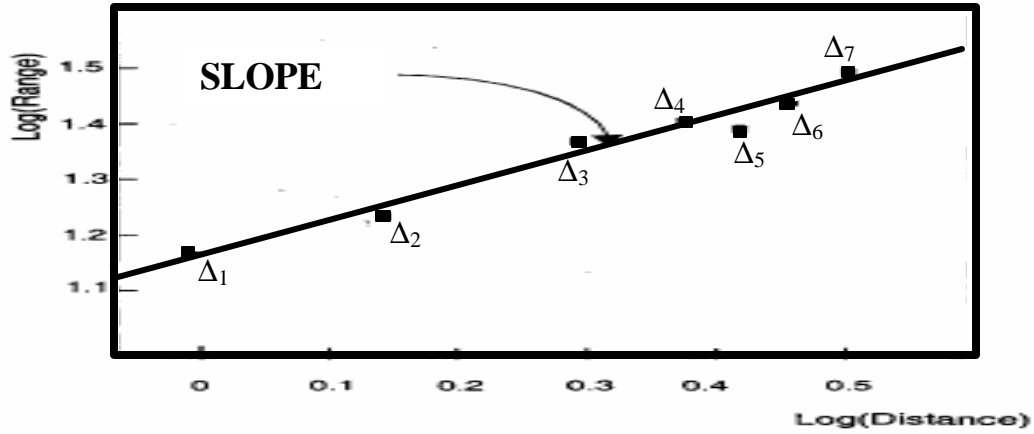


Figure 2.8 Straight line fit to the log(Distance) vs. log(Range) for a 7 pixel wide circular window. The slope is the Hurst coefficient.

The interest images are multispectral images with M bands, so the Hurst coefficient is calculated in each band

$$\mathbf{HC} = \begin{bmatrix} \text{HC}(1) \\ \text{HC}(2) \\ \vdots \\ \text{HC}(M) \end{bmatrix} \quad (2.10)$$

and finally calculated as follows

$$\text{HC} = \|\mathbf{HC}\|_2 \quad (2.11)$$

The size of the circular window is a compromise between the desire to include many pixels values and the need for fast calculation. Similar results are obtained with 5-, 9-, and 11-pixels wide regions [31]. As the window increase in size, more accurate results are achieved but as said before, it's a tradeoff between accuracy and computer consumption.

The straight line fitting will be done using the Hough transform parameter estimation of a straight line. The Hough transform will be used because of its properties of tolerance to noise introduced by the calculation algorithm of the Hurst coefficient and the input image.

### 2.4.3 Peer group coefficient

Peer group coefficient (PGC) is a nonlinear algorithm that gives a quantification of homogeneity in images. PGC was first introduced by Deng *et al.* [32] in 1999 for image smoothing and impulse noise removal in color images. Peer group can be defined as the group of pixels inside a squared overlapping window that are more homogeneous in respect to the central pixel of the window. Using these peer groups a quantification of homogeneity can be calculated for each pixel in the image.

Let  $x_0(n)$  denote an image pixel vector, characterizing the spectral information at position  $n$  centered in a  $w \times w$  squared window. Sort all the pixels in the window according to their distances to  $x_0(n)$  in ascending order and denote the vector as  $x_i(n)$  for  $i = 0, 1, \dots, w^2-1$ . The Euclidean distance measure is used to calculate the distance between all the pixels in the window and the central pixel  $x_0(n)$ .

$$d_i(n) = \|x_0(n) - x_i(n)\|, \quad i = 0, 1, \dots, k = w^2 - 1 \quad (2.12)$$

where  $d_0(n) = d_1(n) = \dots = d_k(n)$ . The peer group  $P(n)$  of size  $m(n)$  for  $x_0(n)$  is defined as

$$P(n) = \{x_i(n), \quad i = 0, 1, m(n) - 1\} \quad (2.13)$$

where  $m(n) = w^2$ . The challenge is to automatically select the peer group size  $m(n)$  for each pixel. Fisher's linear discriminant is used to automatically select the peer group size  $m(n)$  for each pixel in the image.

For two clusters in the squared window, the Fisher's linear discriminant that maximizes the ratio of the inter class scatter to the intra class scatter can be used to separate the two clusters. So, the pixels in the squared window can be divided in two clusters: the peer group cluster and the non-peer group cluster. Since the pixels  $x_i(n)$  are sorted in ascending order according to their distances to  $x_0(n)$ , only the 1D distances are used in the Fisher's discriminant estimation. The criterion to be maximized  $\forall i = 0, 1, \dots, k$  is

$$J(i) = \frac{|a_1(i) - a_2(i)|^2}{s_1^2(i) + s_2^2(i)}, \quad i = 0, 1, \dots, k \quad (2.14)$$

where

$$a_1(i) = \frac{1}{i} \sum_{j=0}^{i-1} d_j(n) \quad (2.15)$$

$$a_2(i) = \frac{1}{k+1-i} \sum_{j=i}^k d_j(n) \quad (2.16)$$

are the sample mean and

$$s_1^2(i) = \sum_{j=0}^{i-1} |d_j(n) - a_1(i)|^2 \quad (2.17)$$

$$s_2^2(i) = \sum_{j=i}^k |d_j(n) - a_2(i)|^2 \quad (2.18)$$

are the sample scatter. The peer group size  $m(n)$  is  $i$  such as it maximize the function

$$m(n) = \arg \max_i J(i) \quad (2.19)$$

The peer group coefficient  $PGC(n)$  is the maximum distance of each peer group

$$PGC(n) = d_{m(n)} - 1 \quad (2.20)$$

## Chapter 3: Procedure

### Preview

The procedures of the four algorithms developed and implemented are discussed in this chapter. The first part discusses the boundary detection algorithm that uses the Hough transform with clustering analysis: new Hough transform for boundary detection. The second part of the chapter discusses the three algorithms used in this work that use the homogeneity computation methods discussed in Chapter 2: local homogeneity analysis which uses the local homogeneity coefficient; Hurst coefficient / Hough transform which uses the Hurst coefficient; and perceptual image quantization which uses the peer group coefficient.

### 3.1 New Hough transform for boundary detection algorithm (NHTBDA)

A reliable segmentation algorithm will help to distinguish between objects under the water and the background. The proposed solution for the problem of image segmentation uses the Hough transform (HT) and clustering information [33]. The HT works as the main method for the segmentation, while clustering information is used a new modality to eliminate false contours in the HT image segmentation, see **Figure 3.1**.

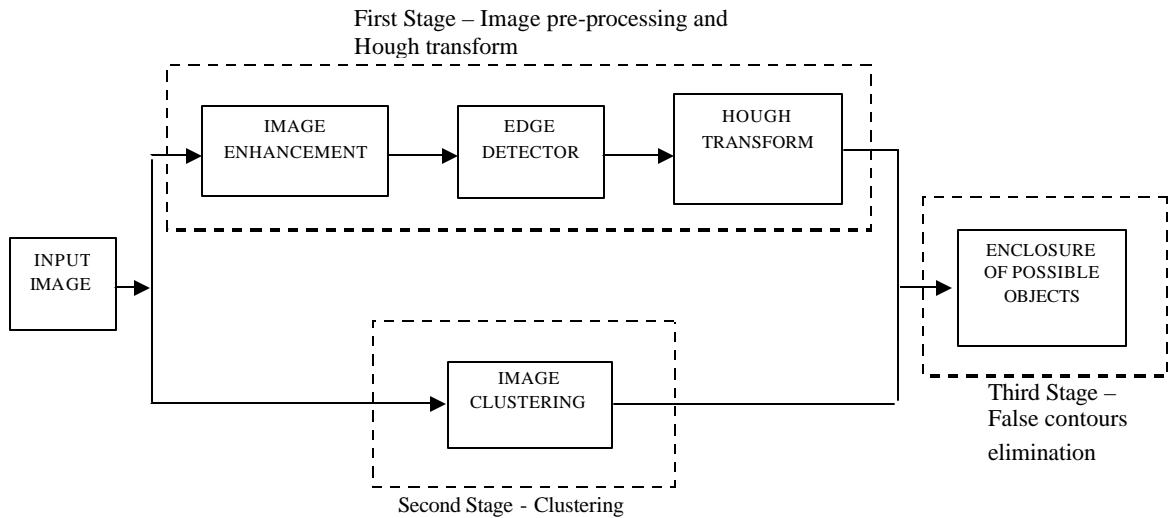


Figure 3.1 Segmentation using the Hough transform for boundary detection

### 3.1.1 First stage-image pre-processing and Hough transform

The first stage of the algorithm consists in the enhancement of the input image, edge detection, and Hough transform calculation.

#### 3.1.1.1 Image enhancement

The input image is filtered for noise removal. Since the edges of the objects in the image can loose contrast with the background, special precaution in filtering the image is needed. A simple 3x3 median filter is used to reduce the noise level in each band of the image.

Next, a histogram equalization on each band of the filtered image is computed (**Figure 3.2**). Histogram equalization enhances the contrast of images by transforming the values in the input intensity image, or the values in the color map of an indexed image, so that the histogram of the output image approximately matches a specified histogram. The main idea of using histogram

equalization is to enhance the contrast between the contour of the object to be segmented and the background so better image detection is achieved.

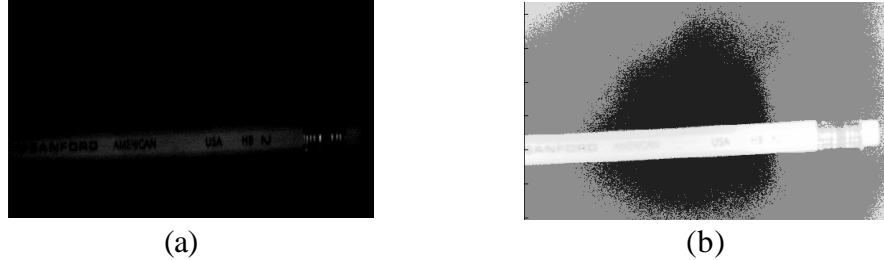


Figure 3.2 Underwater multispectral image of a pencil example: (a) one band of the multispectral pencil image and (b) results after noise removal and histogram equalization of image 3.2a.

### 3.1.1.2 Edge Detector

The edge detector is needed to transform the image used to a binary image with only the edges detected as needed by the HT algorithm. The edge detector takes an intensity image as its input, and returns a black and white binary image of the same size, see **Figure 3.3**. The output image gave 1's where the function finds edges in the input image and 0's elsewhere. The edge detector used was the Sobel detector. The Sobel detector finds edges using the Sobel approximation to the derivative. It returns edges at those points where the gradient of the input image is a maximum.

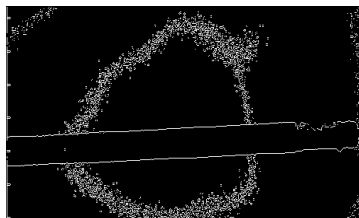


Figure 3.3 Sobel edge detector example result on the enhance image in figure 3.2a

### 3.1.1.3 Hough transform

The Hough transform is performed in the output of the edge detector in each band. The transform is implemented by quantizing the Hough parameter space into finite intervals or accumulator cells. Since the edge detected image is a multispectral image with  $N$  bands, the HT is computed for each band in the image. As the algorithm runs, each  $(x_n, y_n)$  is transformed into a discretized  $(\rho, \theta)$  curve and the accumulator cells, which lie along this curve, are incremented. Each time the HT is computed, an accumulator array is created.  $N$  accumulator arrays are created since there are  $N$  bands in the image. The accumulator arrays are added together to form only one global accumulator array for the whole image, see **Figure 3.4**. Note the infinite line problem.

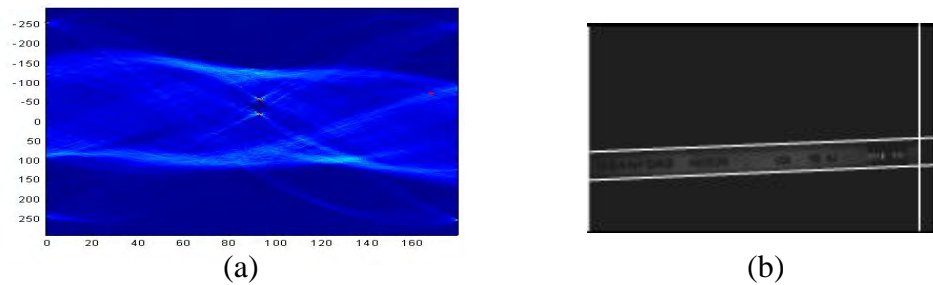


Figure 3.4 Hough transform of the multispectral pencil image: (a) Hough space and (b) Hough transform detected lines

### 3.1.2 Second stage – Clustering

The second stage starts by clustering the input image. Clustering segmentation gives localized information about the desired object that the HT does not have. Fuzzy C-means clustering segmentation technique is used.



### 3.1.2.1 Fuzzy c-means algorithm

The Fuzzy c-means algorithm developed by Besdek [34] from the work of Dunn [35] can be described as follows. The Fuzzy c-means minimize the function  $J$  representing the error within group sum of weighted squares

$$J(U, v) = \sum_{i=1}^c \sum_{k=1}^n (u_{ik})^m \|x_k - v_i\|^2 \quad (3.1)$$

such that

$$\sum_{i=1}^c u_{ik} = 1 \quad (3.2)$$

where  $U$  is the matrix of a fuzzy c-partition of a data set  $X = \{x_1, x_2, \dots, x_n\}$ ,  $n$  the band number,  $v$  is the cluster center vector,  $c$  is the number of clusters,  $u_{ik}$  is the membership value of  $x_k$  to the cluster  $i$ , and  $m$  is the weight exponent. The solution  $v_i$  and  $u_{ik}$  to minimize are obtained by the following steps [36]:

3. Fix  $c$  ( $2 \leq c \leq n$ ), fix  $m$  ( $1 < m < \infty$ ), and initialize the matrix  $U$ .
4. Calculate the cluster center vector  $v_i$  as

$$v_i = \frac{\sum_{k=1}^n (u_{ik})^m x_k}{\sum_{k=1}^n (u_{ik})^m} \quad (3.3)$$

5. Update the membership values  $u_{ik}$  as

$$u_{ik} = \frac{\frac{1}{\|x_k - v_i\|^2} \left( \frac{1}{m-1} \right)}{\sum_{j=1}^c \left( \frac{1}{\|x_k - v_j\|^2} \right)^{\left( \frac{1}{m-1} \right)}} \quad (3.4)$$

6. If parameters changed values significantly, return to 2, otherwise stop.

Clustering result for two clusters of the multispectral image shown in **Figure 3.2a** is shown in **Figure 3.5**.

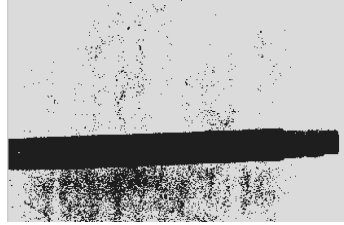


Figure 3.5 Fuzzy c-means results for the multispectral pencil image using two clusters

### 3.1.3 Third stage – False contours elimination

The third stage merges the results from the HT and the cluster analysis of the input image. The information given by the HT is the  $n$  detected lines in the input image that may enclose the desired object. The information given by the cluster analysis is the localization of the desired object. The algorithm to eliminate the false contours (**Figure 3.6**) is as follows:

- 1) Select the cluster where the desired object belongs.
- 2) Find and mark all the intersection points of the HT detected lines.
- 3) For each detected HT line  $j$ , for  $j = 1, 2, \dots, n$ 
  - a. Evaluate a small region around each of the points of HT line  $j$ .
    - i. If the region around the point contains almost all of the pixels (select a threshold) different than the selected cluster, the point of the line is deleted.

- ii. If the region around the point contains almost all of the pixels (select a threshold) equal to the selected cluster, the point of the line is deleted.
  - iii. Else, the point of the line is kept.
- 4) For each detected HT line  $j$ , for  $j = 1, 2, \dots, n$
- a. For each of the kept points of HT line  $j$ 
    - i. Calculate the distance between the kept points and the closest edge point of the selected cluster
    - ii. If the distance is less than a threshold, label the pixels between the point and the closest edge point of the selected cluster as the selected cluster.

### 3.2 Local homogeneity analysis algorithm (LHAA)

Segmentation using local homogeneity analysis uses spatial information that tests for the homogeneity of a given texture pattern in an image with the local homogeneity coefficient [26]. The algorithm proposed for the solution of the image segmentation problem uses a homogeneity analysis for the identification and subdivision of the different regions in the image and a region growing and merging technique to agglomerate similar regions together.

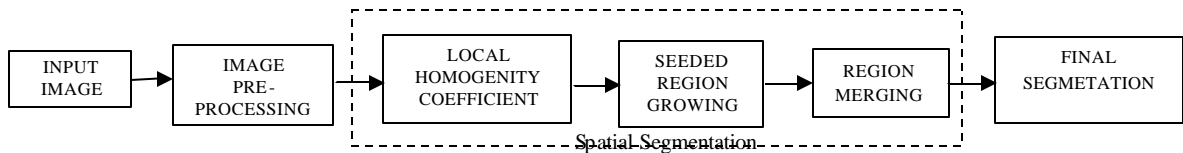


Figure 3.6 Segmentation using local homogeneity analysis algorithm.

### 3.2.1 Image pre-processing

The input image is filtered for noise removal if needed. Since the edges of the objects in the image can loose contrast with the background, special precaution in filtering the image is needed. A simple 3x3 median filter is used to reduce the noise level in the image.

### 3.2.2 Spatial Segmentation

The spatial segmentation consists in the local homogeneity analysis, seeded region growing, and region merging technique.

#### 3.2.2.1 Local homogeneity coefficient

The local homogeneity coefficient (LHC) is calculated for all the pixels in the image. A new image is formed from each of the LHC measured called the homogeneity image (Figure 3.7). The homogeneity image (H-image) is an image whose pixel values are the LHC calculated over local windows centered on those pixels.

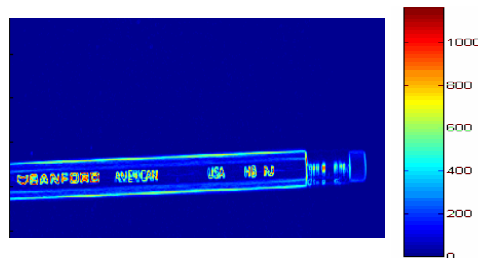


Figure 3.7 H-image for the underwater multispectral image of a pencil using a 3x3 square window.

Remember the LHC has the following characteristics: smaller LHC values if the central pixel is near a homogeneous region and higher LHC values if

central pixel is near a region boundary. So, the characteristics of the H-image make the region growing method very suitable for the subsequent seeded region growing segmentation task.

### 3.2.2.2 Seeded Region growing

Region growing is a bottom-up procedure that starts with a set of seed pixels. The aim is to grow a uniform, connected region from each seed. The algorithm for seeded region growing is as follows:

- 1) Use the same symmetric overlapping window used for calculating the LHC in each pixel of the H-image. Tests for both the global and the local information of the H-image using a threshold  $T_p$

$$T_p = \min \left( \max \left( \mu_p - a_1 \cdot s_p, \mu - a_2 \cdot s \right), \mu + a_3 \cdot s \right) \quad (3.5)$$

where  $(\mu_p, s_p)$  are the mean and variance of the intensities in the symmetric overlapping window in the H-image,  $(\mu, s)$  are the mean and the variance of the intensities of all H-image, and  $a_1, a_2, a_3$  are constant.

- 2) For each pixel evaluated in the H-image determine if it is a seed

$$\text{Pixel } (x_c, y_c) \text{ in H-image} \quad \left\{ \begin{array}{ll} \text{Seed,} & H(x_c, y_c) \leq T_p \\ \text{Not a seed,} & \text{else} \end{array} \right. \quad (3.6)$$

- 3) Connect the seeds using 8-connectivity and obtain seeds regions and remove the holes in the seed regions.
- 4) Grow the region assigning unlabeled pixels to the neighbor seed (one by one).

Over segmentation often occurs as a result of the seeded region growing. The result after seeded region growing of the underwater multispectral image of a pencil is shown in **Figure 3.8**.

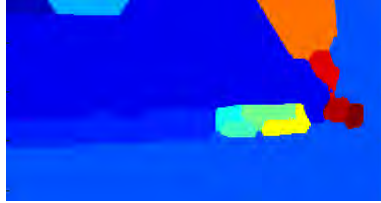


Figure 3.8 Over segmented seeded region growing of the underwater multispectral image of a pencil.

### 3.2.2.3 Region merging

The output segmentation after seeded region growing is often over segmented, which makes the region merging often necessary. Merge the over segmented regions using an agglomerative method [37]. The closest centroids of the regions are merged together in one region. Contiguous region has highest priority in the merging of the regions. The merging process continues until a threshold for the distances between centroids is reached.

## 3.3 Hurst coefficient / Hough transform algorithm (HCHTA)

Segmentation using the Hurst coefficient (HC) with Hough transform uses spatial information that tests for the homogeneity of a given texture pattern in an image with the Hurst coefficient using the Hough transform for linear fitting. The Hough transform is used as a new modality for the calculation of the Hurst coefficient. The algorithm proposed and implemented (**Figure 3.9**) for the

solution of the image segmentation problem uses the Hurst coefficient with the Hough transform for local homogeneity quantification, weighted c-means is used to make a class map of the image, and finally, local homogeneity analysis algorithm is performed in this class map.

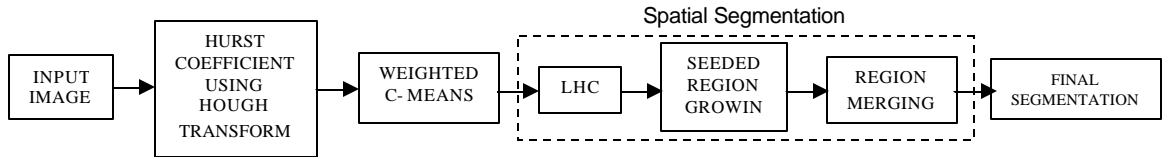


Figure 3.9 Segmentation using Hurst coefficient / Hough transform algorithm

The usage of the Hurst coefficient using the Hough transform is intended to give a new sense of multiscale homogeneity quantification of a pixel and its neighbors that the local homogeneity analysis does not have. Hurst coefficient calculation is proposed and implemented before the local homogeneity analysis algorithm.

### 3.3.1 Hurst coefficient using the Hough transform

The Hurst coefficient (HC) is calculated for all the pixels in the image. The Hough transform is used to perform straight line fit of the  $\log(\text{range})$  and  $\log(\text{distance from center})$ . The slope of this line is the Hurst coefficient. The Hough transform is chosen to perform straight line fit over other straight line fitting like least square because of its tolerance to noise. The Hurst coefficient (HC) using the Hough transform is calculated for all the pixels in the image for the measurement of the local homogeneity (**Figure 3.10**).

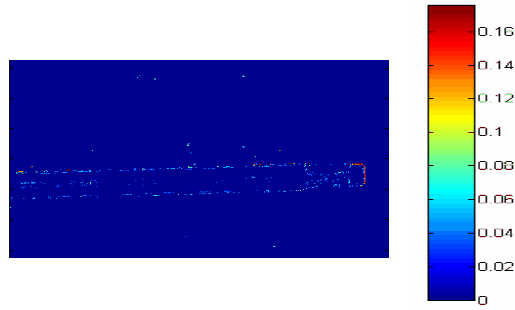


Figure 3.10 Hurst coefficient using the Hough transform image of a pencil using 7x7 circular window.

### 3.3.2 Weighted c-means

A weighted version of the c-means algorithm is performed on the image to create a class map of the image. The weight of each pixel is calculated by

$$v(n) = e^{-HC(n)} \quad (3.7)$$

Pixels in smooth regions are weighted more than in noisy regions. The weighted image is shown in **Figure 3.11**.



Figure 3.11 Weighted image of Hurst coefficient using the Hough transform of a pencil using a 7x7 circular window.

Using the pixels weights, the weighted c-means clustering algorithm is as follows:



- 1) Choose the number of clusters  $i$  in the image and some initial values for the cluster means  $\mathbf{c}$ .
- 2) Classify the  $n$  samples by assigning them to the class of the closest mean using the weighted Euclidean distance classifier

$$g_i = v(n)(\mathbf{X}_n - \mathbf{c}_i)^T (\mathbf{X}_n - \mathbf{c}_i) \quad (3.8)$$

Then the pixel  $\mathbf{X}_n$  is assigned to a cluster  $i$  if the following rule is accomplished

$$g_i(\mathbf{X}_n) \leq g_j(\mathbf{X}_n) \quad \forall j \rightarrow \mathbf{X}_n \in \mathbf{c}_i \quad (3.9)$$

- 3) Recompute the means as the weighted average of the samples in their class

$$\mathbf{c}_i = \frac{\sum_{k=1}^n v(n)\mathbf{X}_n}{\sum_{k=1}^n v(n)} \quad (3.10)$$

where  $n$  is the number of pixels in the  $i^{\text{th}}$  cluster. The means are shifted towards the regions with higher weights (smooth regions).

- 4) If any mean's value changed significantly go to step 2, otherwise stop.

### 3.3.3 Spatial Segmentation

The class map of the image calculated using weighted c-means is the input to the spatial segmentation that consists in the same parts as the spatial segmentation discussed in the local homogeneity analysis algorithm: local homogeneity coefficient (LHC), seeded region growing, and region merging. Spatial segmentation is achieved in the same manner as **Section 3.2.2**.

### 3.4 Perceptual image quantization algorithm (PIQA)

Segmentation using perceptual image quantization uses spatial information that tests for the homogeneity of a given texture pattern in an image with peer group coefficient (PGC) [38]. The algorithm proposed (**Figure 3.12**) for the solution of the image segmentation problem uses PGC for local homogeneity quantification, weighted c-means is used to make a class map of the image, and finally, local homogeneity analysis algorithm is performed in this class map.

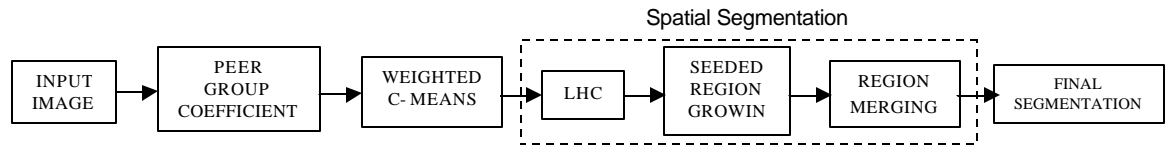


Figure 3.12 Segmentation using the perceptual image quantization algorithm

#### 3.4.1 Peer group coefficient

The peer group coefficient (PGC) is calculated for all the pixels in the image for the measurement of the local homogeneity (**Figure 3.13**).

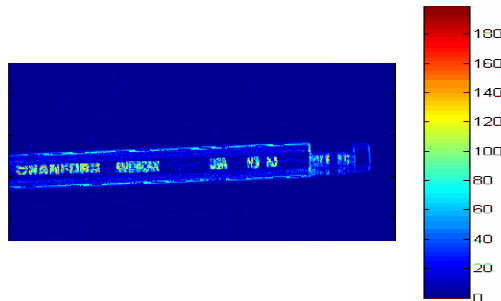


Figure 3.13 Peer group coefficient image of a pencil using a 3x3 square window.

### 3.4.2 Weighted c-means

A weighted version of the c-means algorithm is performed on the image to create a class map of the image. The weight of each pixel is calculated by

$$v(n) = e^{-PGC(n)} \quad (3.11)$$

and the weighted image is shown in **Figure 3.14**.

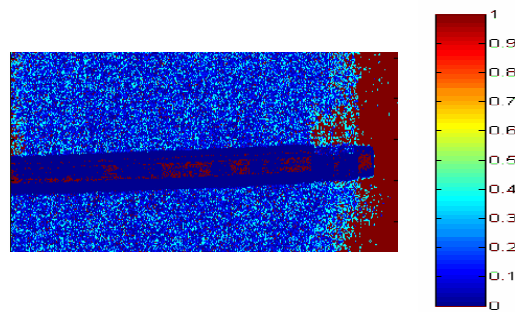


Figure 3.14 Weighted image of peer group coefficient of a pencil using a 3x3 square window.

Pixels in smooth regions are weighted more than in noisy regions. The weighted c-means algorithm is then calculated as **Section 3.3.2**.

### 3.4.3 Spatial segmentation

The class map of the image calculated using weighted c-means is the input to the spatial segmentation that consists in the same parts as the spatial segmentation discussed in the local homogeneity analysis algorithm: local homogeneity coefficient (LHC), seeded region growing, and region merging. Spatial segmentation is achieved in the same manner as **Section 3.2.2**.

## Chapter 4: Results

### Preview

The results of the algorithms implemented and developed are discussed in this chapter. Chapter 4 is divided in three parts depending on the types of images used in the experiments. The first part of the chapter discusses the underwater multispectral images generated in a controlled environment and the results of the algorithms for this type of images. The second part of the chapter discusses the underwater multispectral images taken by an Autonomous Underwater Vehicle (AUV) and the results of the algorithms for this type of images. The third part of the chapter discusses the remotely sensed images and the results of the algorithms for this type of images.

### 4.1 Underwater multispectral images generated in a controlled environment

The synthetic underwater multispectral images were taken by a CCD camera coupled with a spectral filter in a controlled environment.

#### 4.1.1 First image: pencil

The details of the first synthetic multispectral underwater image are given in **Table 4.1** and a visualization of the first band (500 nm) is given in **Figure 4.1**. The image consists only of a pencil submerged in 20.32 cm. of water with

scattering and the background. Due to the illumination, shadows are formed at the edges of the pencil which breaks the contour of the pencil.

Table 4.1 Details of the first multispectral underwater image generated in a controlled environment: pencil

Image Name	Bits per pixel	Number of spectral bands	Wavelength range (nm)	Spectral Resolution (nm)
Pencil	8	22	500 - 650	15

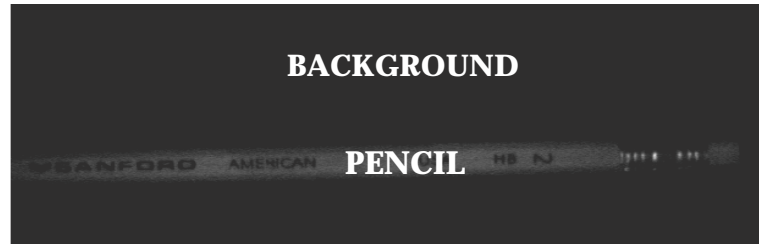
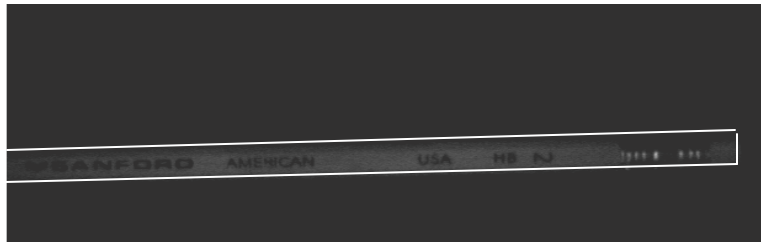
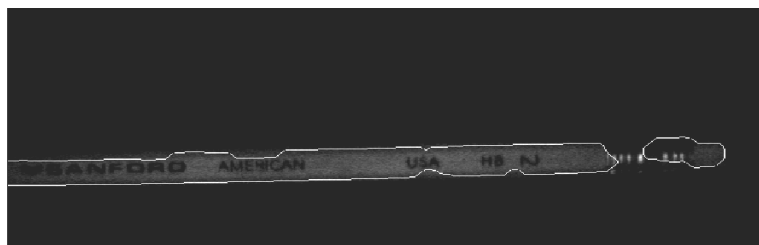


Figure 4.1 First underwater multispectral image generated in a controlled environment: pencil.

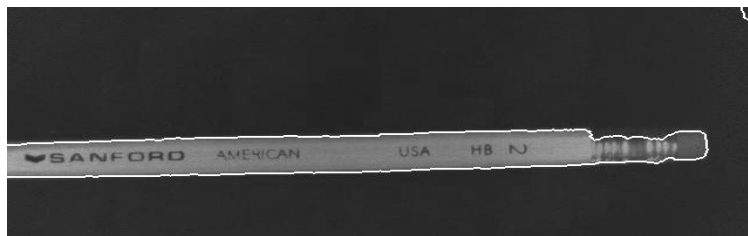
The results of the segmentation algorithms using this image are given in **Figure 4.2**. The results show that the new Hough transform for boundary detection **Figure 4.2a** gives the better segmentation for the pencil image. As can be seen from the original image in **figure 4.1**, the contour of the pencil is broken and shadows are formed at the edges due to the lack of illumination. The new Hough transform for boundary detection reconstruct the broken boundaries due to the fact that each collinear point in the broken boundaries of the pencil contributes to the global solution. The segmentation using the Hurst coefficient / Hough transform (**Figure 4.1c**) and perceptual image quantization (**Figure 4.1d**)



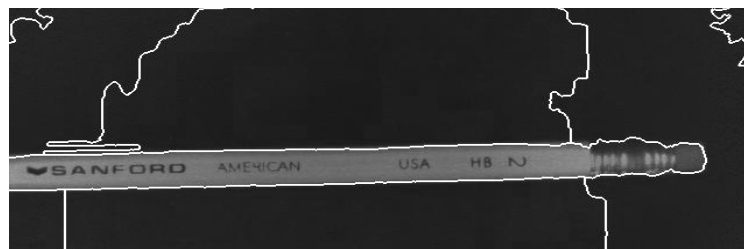
(a)



(b)



(c)



(d)

Figure 4.2 Segmentation results of the first image using: (a) new Hough transform for boundary detection, (b) local homogeneity analysis, (c) Hurst coefficient / Hough transform, and (d) perceptual image quantization.

gives a good and similar segmentation results with more visualization of the noise regions due to the illumination. The segmentation result using local homogeneity analysis (**Figure 4.2b**) gives the more inaccurate segmentation for the pencil. The region of the background invades the pencil region that can be due to the shadows and the lack of contrast in the boundaries of the pencil.

#### 4.1.2 Second image: nut

The details of the second synthetic multispectral underwater image are given in **Table 4.2** and a visualization of the first band (500 nm) is given in **Figure 4.3**. The image consists only of an iron nut submerged in 20.32 cm. of water with scattering and the background.

Table 4.2 Details of the second multispectral underwater image generated in a controlled environment: nut

<b>Image Name</b>	<b>Bits per pixel</b>	<b>Number of spectral bands</b>	<b>Wavelength range (nm)</b>	<b>Spectral Resolution (nm)</b>
<b>Nut</b>	8	22	500 - 650	15



Figure 4.3 Second underwater multispectral image generated in a controlled environment: nut.

The results of the segmentation algorithms using this image are given in **Figure 4.4**.

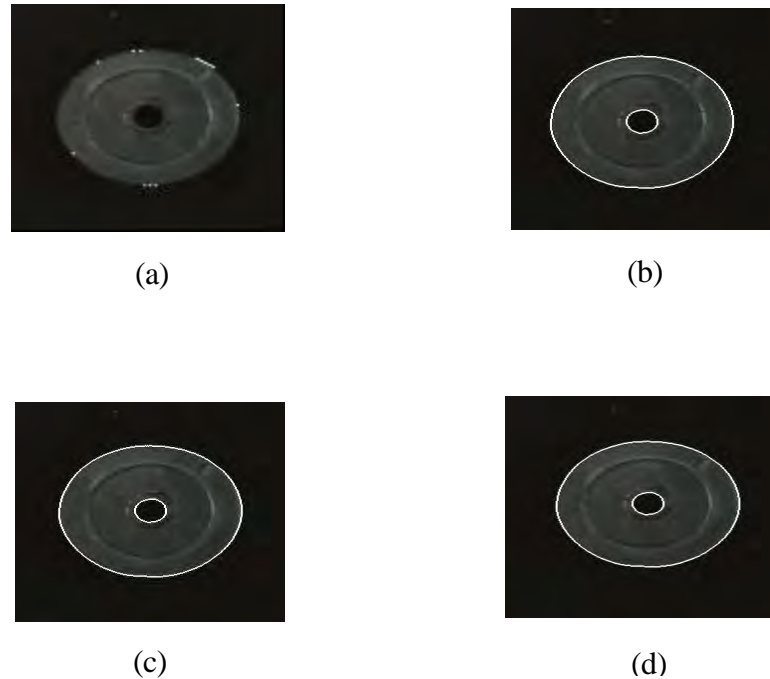


Figure 4.4 Segmentation results of the second image using: (a) new Hough transform for boundary detection, (b) local homogeneity analysis, (c) Hurst coefficient / Hough transform, and (d) perceptual image quantization.

The results show that the new Hough transform for boundary detection **Figure 4.4a** gives the worst segmentation for the nut image. The error in the segmentation is because the nut is a circular object. The edges of the nut do not add up in the Hough transform analysis giving error in the line approximation. Since the Hough transform is used for the estimation of lines, problem using this method arisen with amorphous and circular objects. The segmentation using local homogeneity analysis (**Figure 4.4b**), the Hurst coefficient / Hough transform (**Figure 4.4c**) and perceptual image quantization (**Figure 4.4d**) gives a



perfect segmentation. Similar segmentations are achieved since there is not great variability textually and spectrally.

#### 4.1.3 Third image: tank bottom with objects

The details of the third multispectral underwater image are given in **Table 4.3** and RGB visualization is given in **Figure 4.5**. The image consists in 4 known objects and two types of background submerged in 45.72 cm. of water with scattering.

Table 4.3 Details of the third multispectral underwater image generated in a controlled environment: tank bottom with objects

<b>Image Name</b>	<b>Bits per pixel</b>	<b>Number of spectral bands</b>	<b>Wavelength range (nm)</b>	<b>Spectral Resolution (nm)</b>
<b>Tank Bottom with objects</b>	8	33	400 - 720	10

The four known objects in the image are: dead coral, leaves, lead weight, and rock with two types of background: yellow and black. As can be seen for **Figure 4.3**, each object has a great variability textually and spectrally. This can be seen especially in the leaves, rock, and weight and it surely will affect the results. It can be noted also that the rock and some leaves have similar spectral response.

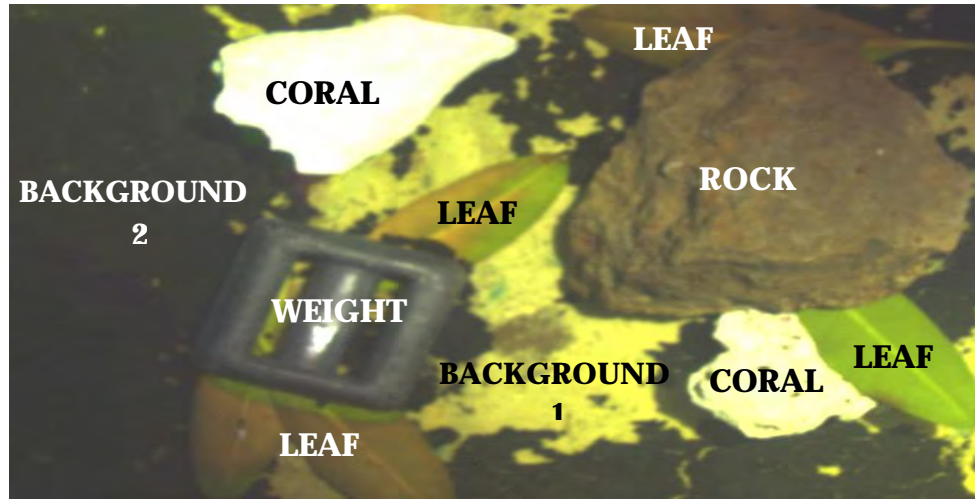
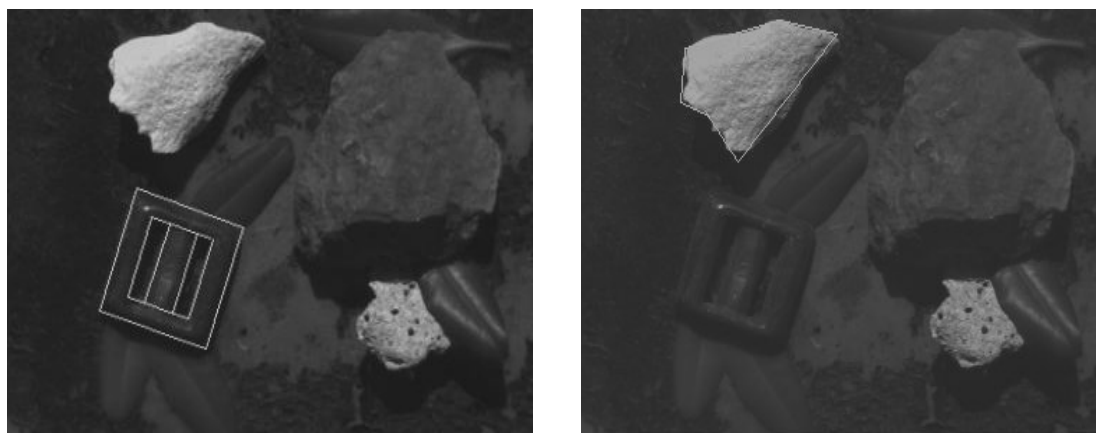
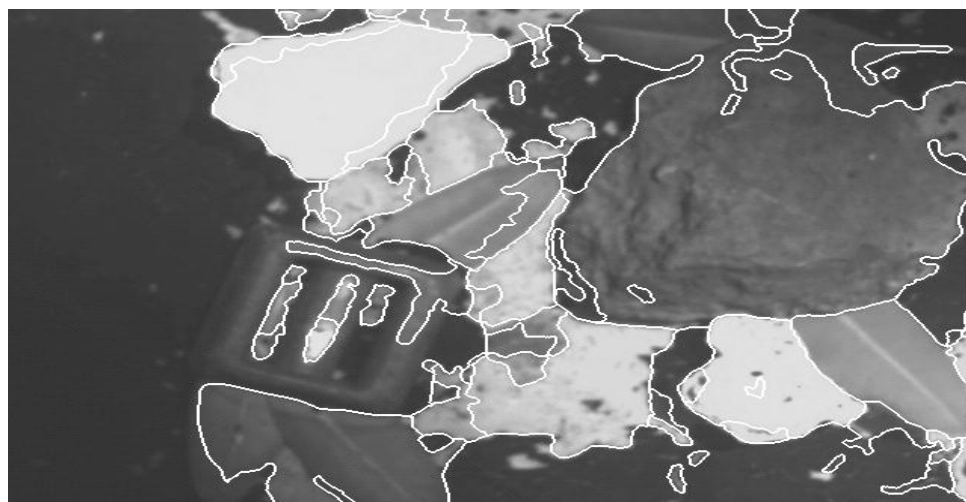


Figure 4.5 Third underwater multispectral image generated in a controlled environment RGB visualization: tank bottom with objects.

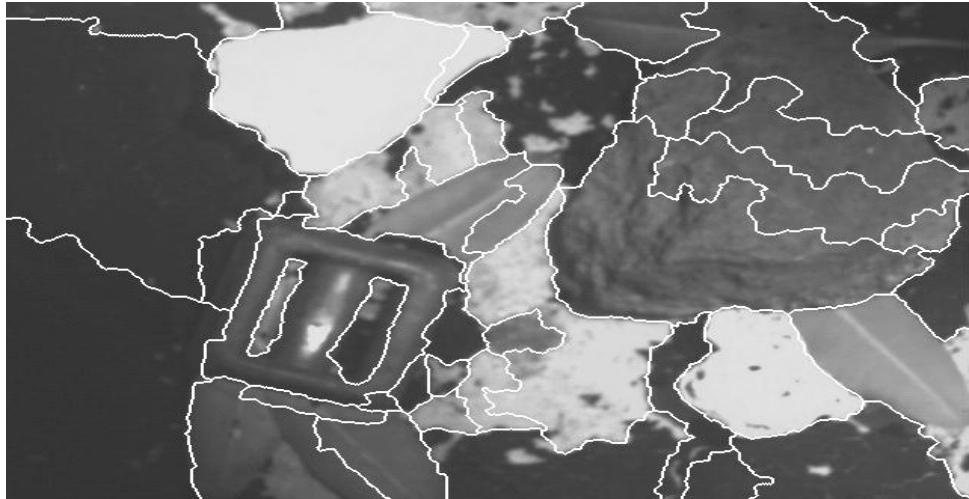
The results of the segmentation algorithms using this image are given in **Figure 4.6**. The segmentation using the new Hough transform for boundary detection denotes great problem coping with rich in both spectral variability and texture scenes. Doing the segmentation of the image by parts, good results can be achieved (**Figure 4.6a**) in low varying shapes only. Remember that the Hough transform is used for estimations of lines. The segmentation is achieved for the lead weight and the upper dead coral only since are the more regular and linear objects in the images. The segmentation using the Hurst coefficient/Hough transform (**Figure 4.6c**) and the perceptual image quantization (**Figure 4.6d**) gave the best results. The Hurst coefficient/Hough transform gave a more coarse segmentation in comparison to the perceptual image quantization, leaving small details, especially in the backgrounds, inside other regions. The perceptual image



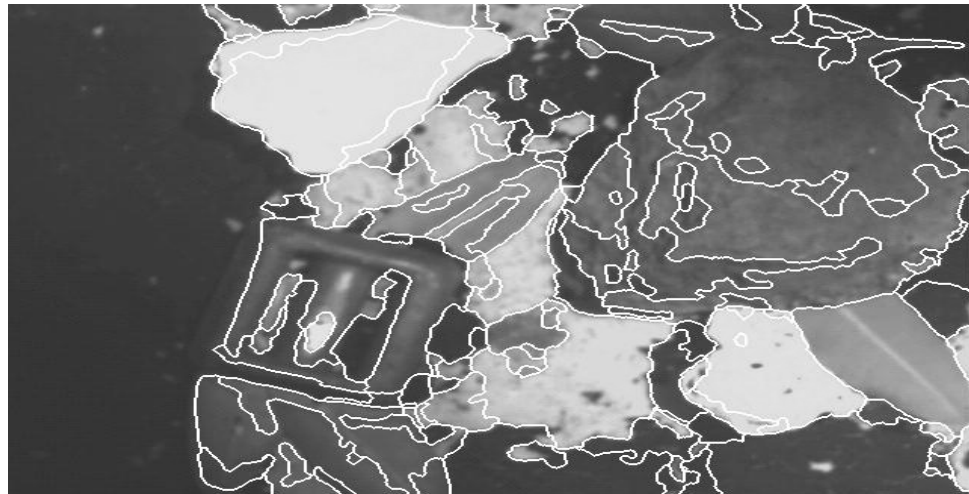
(a)



(b)



(c)



(d)

Figure 4.6 Segmentation results of the second synthetic image using: (a) new Hough transform for boundary detection, (b) local homogeneity analysis, (c) Hurst coefficient / Hough transform, and (d) perceptual image quantization.

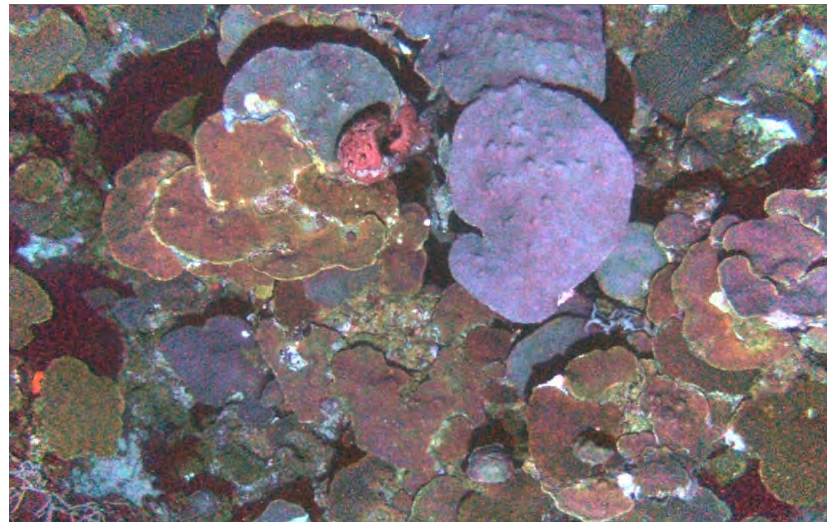
quantization gave more detailed segmentation as can be seen in the separation of background 1 from background 2 and the separation in different regions inside the objects with great variability like the rock and the weight. The segmentation using local homogeneity analysis (**Figure 4.6b**) gave the coarsest segmentation that cannot separate certain objects like the weight and the background 2.

## 4.2 Underwater multispectral image taken by an Autonomous Underwater Vehicle (AUV)

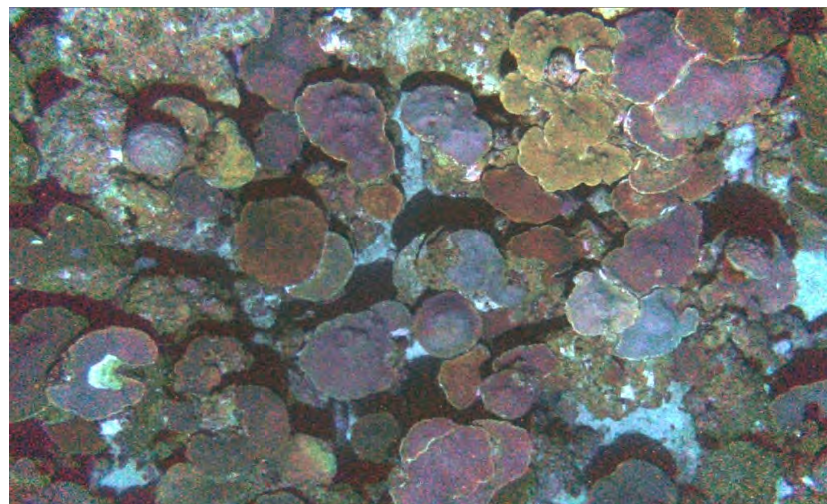
The underwater multispectral images were taken using an automated underwater vehicle (AUV) at the Hind Bank Marine Conservation District (MCD), south of Saint Thomas, United State Virgin Island at approximately 40 meters depth. The camera to substrate distance was approximately 3.5 meters. A set of almost 6000 AUV images were acquired at this site. The details of the AUV multispectral image are given in **Table 4.4** and RGB visualization is given in **Figure 4.7**.

Table 4.4 Details of the underwater multispectral image taken by an AUV

<b>Image Name</b>	<b>Bits per pixel</b>	<b>Number of spectral bands</b>	<b>Wavelength range (nm)</b>	<b>Spectral Resolution (nm)</b>
<b>AUV</b>	8	3	RGB image	



(a)



(b)

Figure 4.7 Two underwater multispectral RGB images taken by an AUV

The AUV images have low contrast, and are very noisy. The subsurface images are extremely rich in both spectral variability and texture, making the segmentation very difficult. So, the main task is to divide the images in homogeneous regions. Since large shape variability exist in the images, the Hough transform is not performed.



A classification map of only one underwater multispectral image taken by an AUV (**Figure 4.7a**) was done using the software Canvas 8.0.3 (**Figure 4.8**). Canvas is a software used to acquire the regions of interest in an image using polygon approximation of the regions drawn by hand<sup>1</sup>. A marine biologist may spend many hours in classifying the corals in all 6000 images with this software. The segmentation algorithms researched and developed here can be used to help the marine biologist in the classification of these types of images.

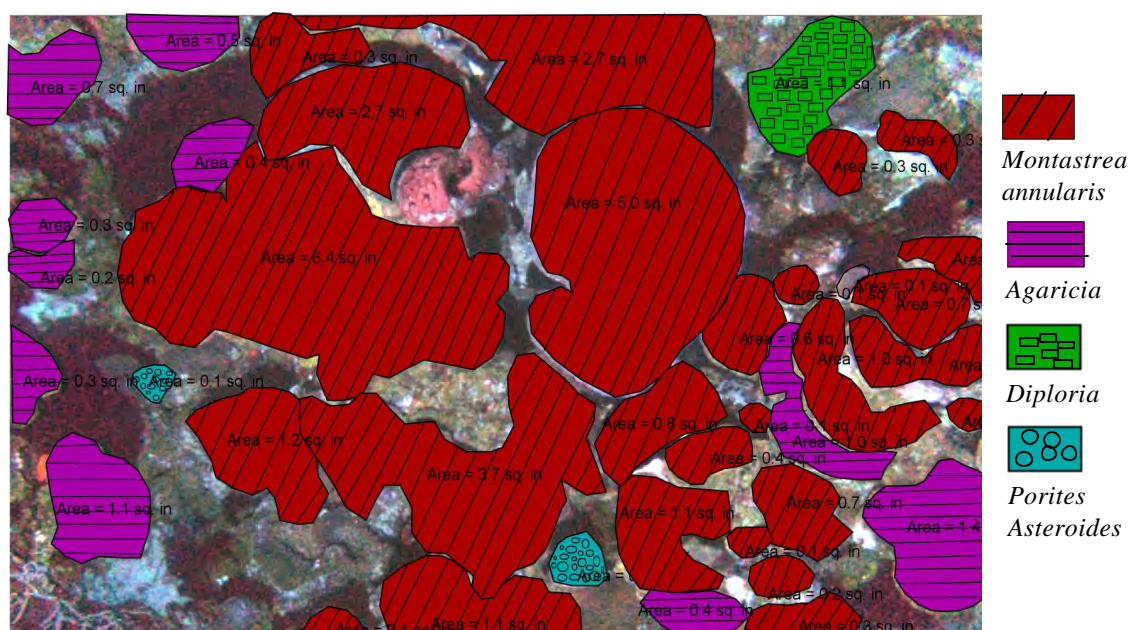
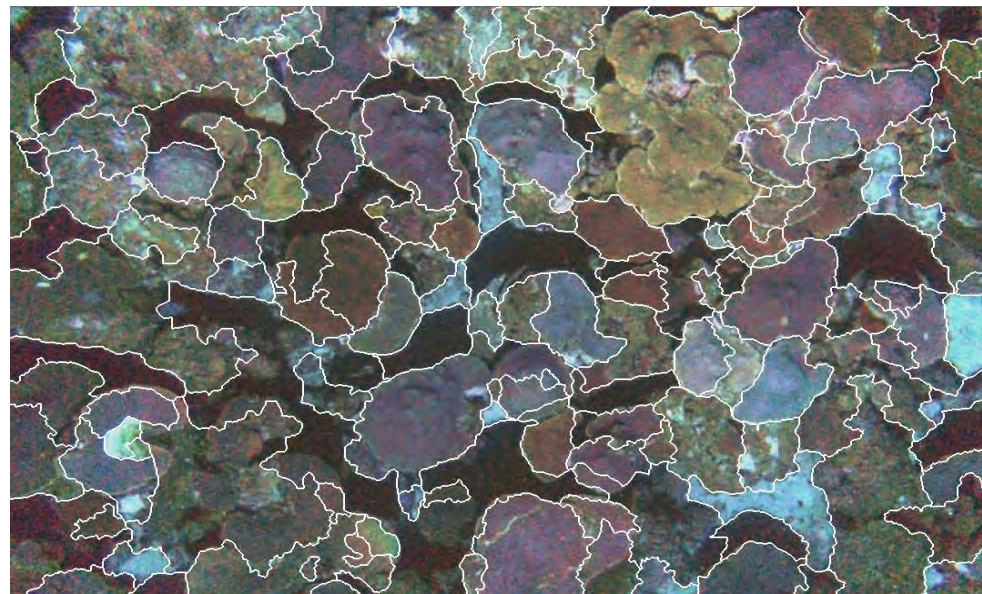
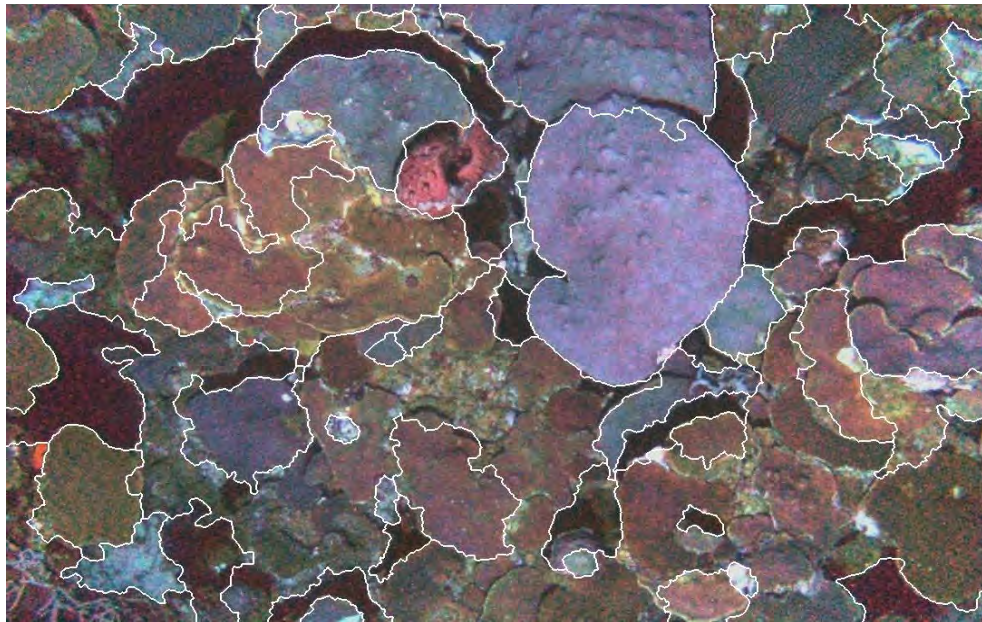


Figure 4.8 Classification map of the underwater multispectral image taken by an AUV using Canvas 8.0.3<sup>1</sup>

The classification map shows a predominant coverage of the *Montastrea annularis* (complex) coral reef among with *Agaricia*, *Diploria*, and *Porites astreoides* species.

<sup>1</sup> Classification of the AUV images using Canvas 8.0.3 was done by hand by Juan Torres.

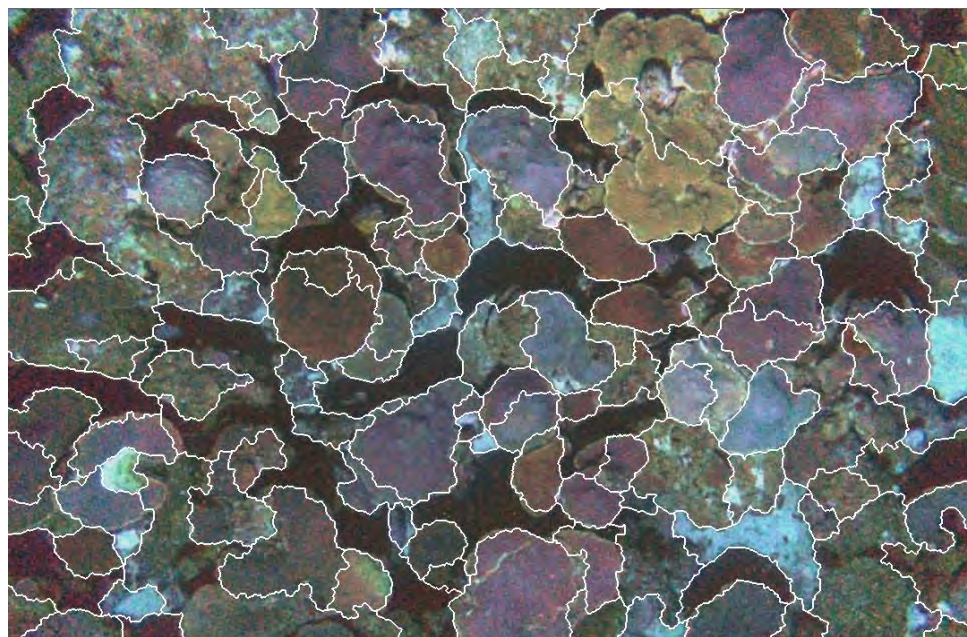
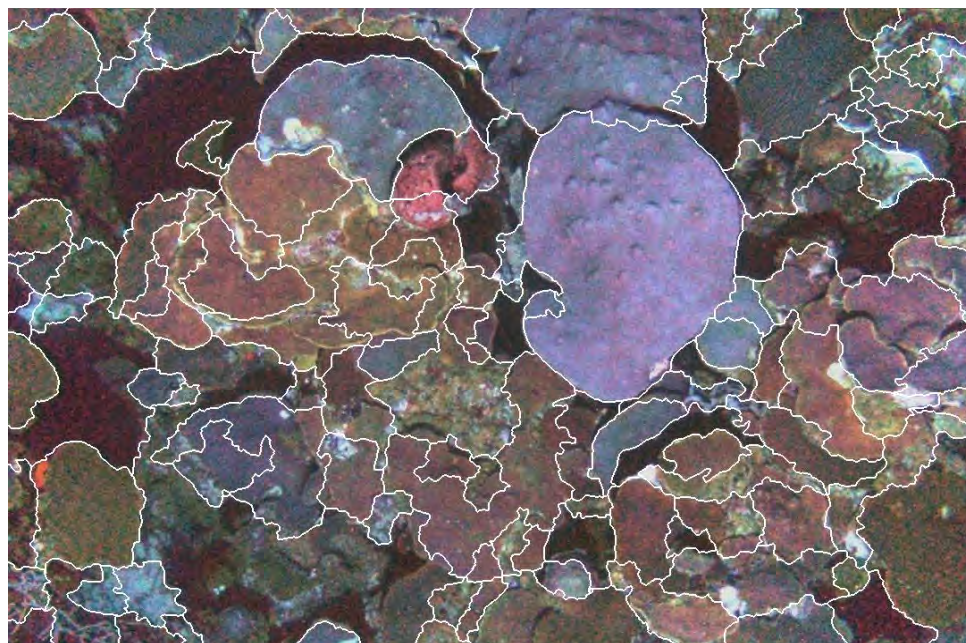
The results of the segmentation algorithms using both AUV images are given in **Figure 4.9**.



(a)

Figure 4.9a Segmentation results of both AUV image using local homogeneity analysis.

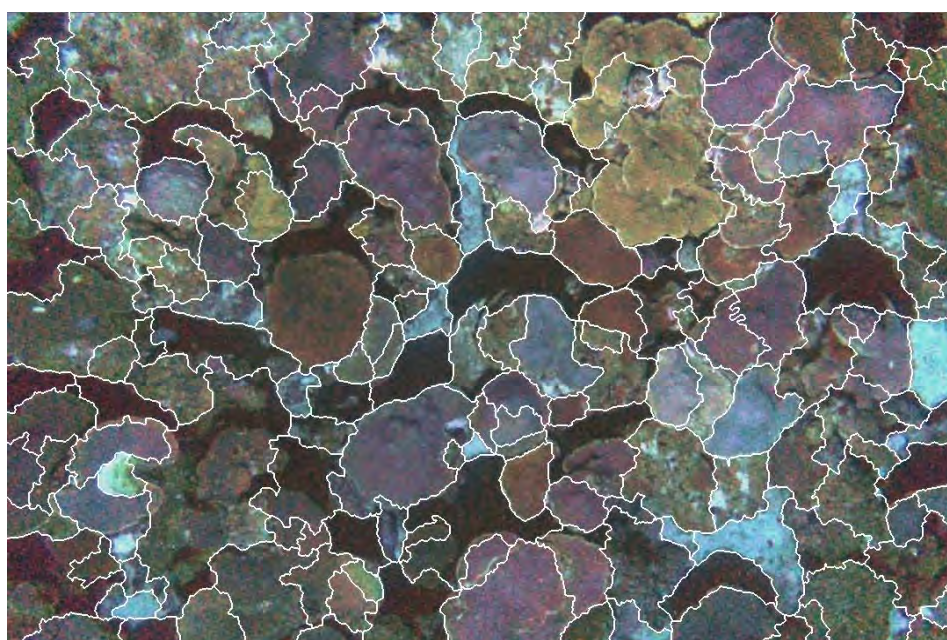
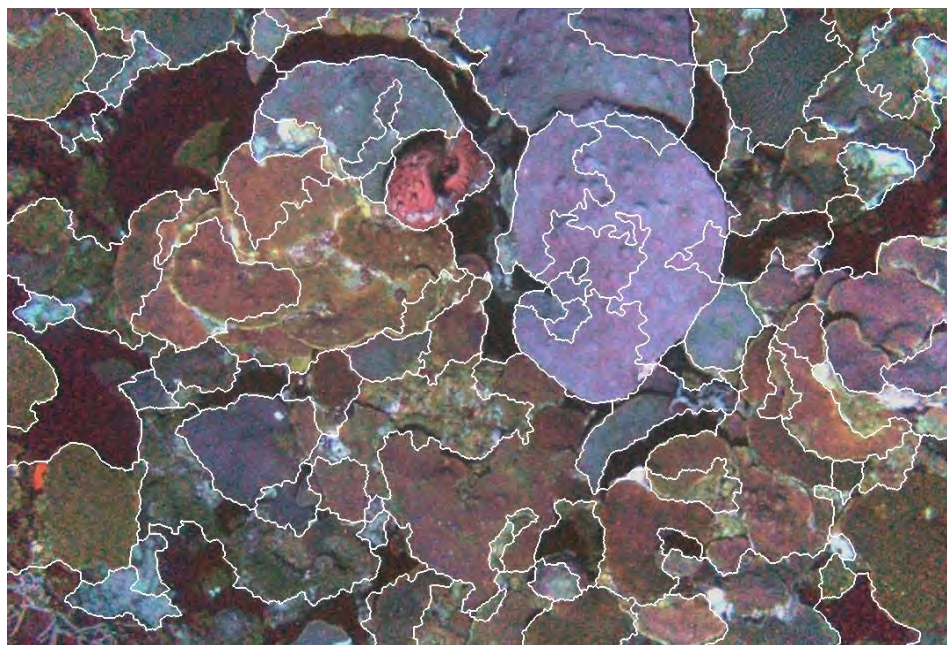




(b)

Figure 4.9b Segmentation results of both AUV image using Hurst coefficient / Hough transform





(c)

Figure 4.9c Segmentation results of both AUV image using perceptual image quantization.

The visual inspection for the evaluation of the segmentation of the algorithms is very difficult due to the extremely variability in shape, texture, and spectral response. Basically, all three algorithms performed very well in the identification of the homogeneous regions. Again, the coarsest segmentation is given by the local homogeneity analysis (**Figure 4.9a**). Comparing visually the results of the Hurst coefficient/Hough transform (**Figure 4.9b**) and the perceptual image quantization (**Figure 4.9c**), the best results is achieved by the Hurst coefficient/Hough transform because it gives a better separation of the homogeneous regions in the images. Doing a meticulous comparison of the segmentation given by this algorithm in the first AUV image with class map and the class map in **Figure 4.8**, each of the corals regions detected in the class map is detected in the segmented image. The region that had the most problem is the area around the *Diploria* coral. The area is very noisy and had very low contrast.

To further extent the analysis, another region merging algorithm is used to merge the regions detected in another set of AUV images with class maps (**Figure 4.10**). A supervised region merging is used using training samples for the corals detected in the class maps for the classification of the regions. The supervised region merging used the centroids of the training samples to classify the regions that are closest to each centroid of the training samples. Each homogeneity algorithm is performed using the same criteria in the classification.



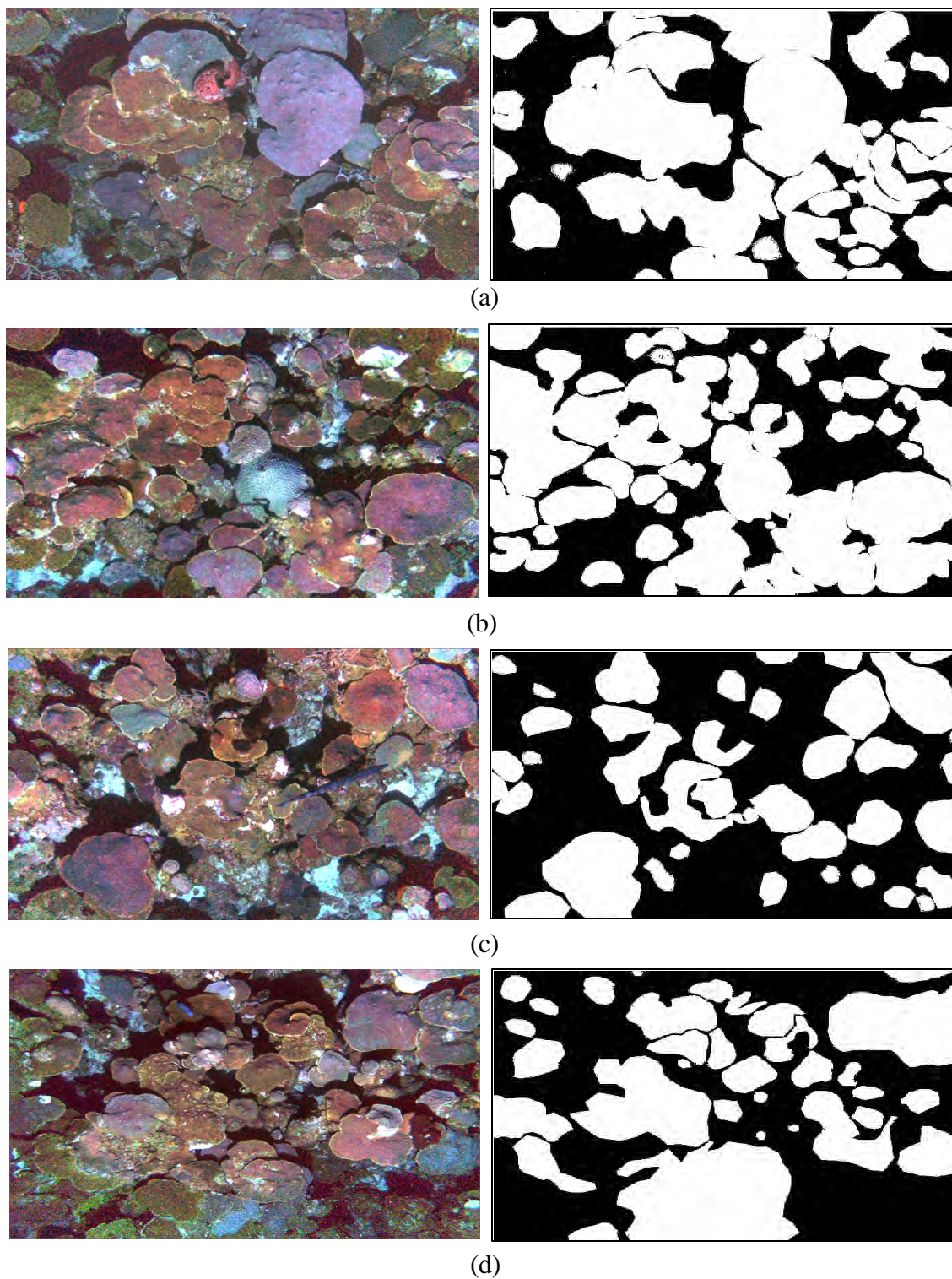


Figure 4.10 Set of AUV images with class maps done in Canvas. In the class maps, the corals regions are in white and background regions are in black.

The number of pixels of each class (coral and background) of the class maps of the image in **Figure 4.10** is summarized in **Table 4.5**.

Table 4.5 Composition of classes of each image of Figure 4.10

	<b>Number of Pixels</b>			
	<b>Figure 4.10a</b>	<b>Figure 4.10b</b>	<b>Figure 4.10c</b>	<b>Figure 4.10d</b>
<b>Pixels Corals</b>	479475	175154	315397	616508
<b>Pixels Background</b>	303169	98766	467247	694212
<b>Total pixels</b>	782644	273920	782644	1310720

The classification results of each image in **Figure 4.10** using the homogeneity based algorithms are compared with the true classification class maps done in Canvas and the results are summarized in **Table 4.6, 4.7, 4.8** and **4.9**. The percentage of correct classification between the classification results and the true class map of corals and background are presented as well as an overall performance that is the percentage of correct classification between the classification results and the true class map.

Table 4.6 Classification results of Figure 4.10a

<b>Figure 4.10a</b>	<b>Percentage Pixels Detected in Correct Classification</b>		
	<b>LHA</b>	<b>HCHTA</b>	<b>PIQA</b>
<b>Pixels Corals</b>	65.67 %	69.66 %	66.43 %
<b>Pixels Background</b>	78.01 %	80.04 %	77.35 %
<b>Overall Performance</b>	70.01 %	73.68 %	70.79 %

Table 4.7 Classification results of Figure 4.10b

<b>Figure 4.10b</b>	<b>Percentage Pixels Detected in Correct Classification</b>		
	<b>LHA</b>	<b>HCHTA</b>	<b>PIQA</b>
<b>Pixels Corals</b>	48.71 %	72.28 %	55.54 %
<b>Pixels Background</b>	84.78 %	63.78 %	69.95 %
<b>Overall Performance</b>	70.24 %	67.21 %	60.74 %

Table 4.8 Classification results of Figure 4.10c

<b>Figure 4.10c</b>	<b>Percentage Pixels Detected in Correct Classification</b>		
	<b>LHA</b>	<b>HCHTA</b>	<b>PIQA</b>
<b>Pixels Corals</b>	65.14 %	72.28 %	48.71 %
<b>Pixels Background</b>	66.87 %	63.78 %	84.78 %
<b>Overall Performance</b>	66.18 %	67.21 %	70.24 %

Table 4.9 Classification results of Figure 4.10d

<b>Figure 4.10d</b>	<b>Percentage Pixels Detected in Correct Classification</b>		
	<b>LHA</b>	<b>HCHTA</b>	<b>PIQA</b>
<b>Pixels Corals</b>	72.48 %	70.23 %	67.02 %
<b>Pixels Background</b>	63.54 %	70.86 %	67.20 %
<b>Overall Performance</b>	67.74 %	70.57 %	67.12 %

Comparing the results of the classifications for the images of Figure 4.10, the HCHTA gave the higher percentages in the detection of corals and

background. The percentage of detected coral pixels for each image is around a constant ~70% for the HCHTA. Due to the variability of the classes shown in the class map, it's difficult to classify all the regions using a small set of pixels for the training samples and the centroids of the regions and the training samples. The LHA and PIQA performed well also but with lower percentage of classification compared to the HCHTA.

The result of **Figure 4.10a** using the Hurst coefficient/Hough transform is shown **Figure 4.11**. There are 411 different regions in this image.

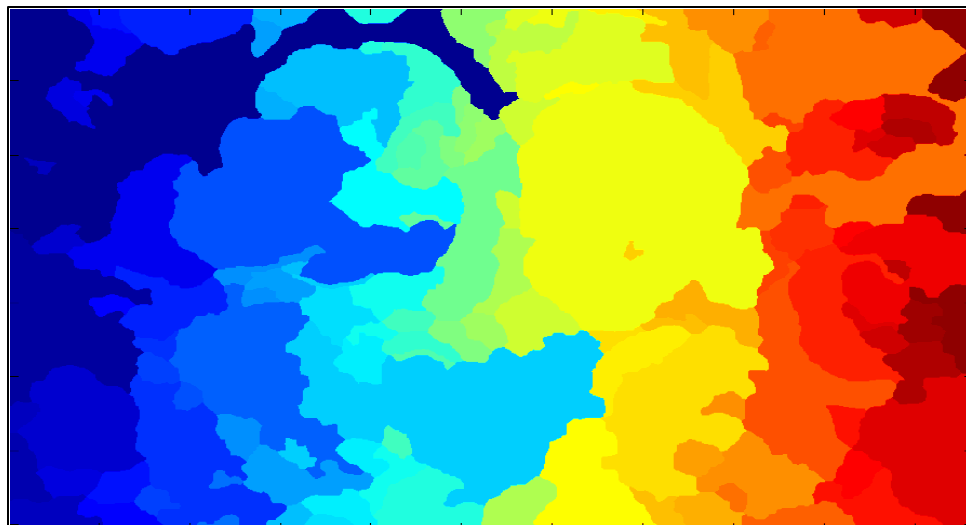


Figure 4.11 Region growing result of Hurst coefficient/Hough transform with 451 regions

Using the training samples of the corals, the desired coral regions are detected and classified (**Figure 4.12**).



Figure 4.12 Classification of the corals using the supervised merging algorithm on the region growing result of Hurst coefficient/Hough transform

The classification results gave 69.66% classification of the coral and 80% for the background for an overall performance of 73.68%.

### 4.3 Remotely sensed underwater multispectral image

The satellite multispectral image was taken by the IKONOS sensor over southwestern of Puerto Rico at La Parguera. The multispectral image was corrected atmospherically. The details of the IKONOS image are given in **Table 4.10** and RGB visualization is given in **Figure 4.13**. The area of interest in La Parguera is the Enrique Reef that is approximately 1.1 km. long.

Table 4.10 Details of the remotely sensed underwater multispectral image taken by IKONOS

Image Name	Bits per pixel	Number of spectral bands	Wavelength range (nm)	Spectral Resolution (nm)	Spatial Resolution (m)
IKONOS	11	4	450 - 770	120	1





Figure 4.13 RGB visualization of IKONOS image of La Parguera, Enrique Reef denoted.

The area of Enrique Reef in the IKONOS image is zoomed and shown in **Figure 4.14**.



Figure 4.14 RGB visualization of IKONOS image of Enrique reef area

A classification map of Enrique Reef area is shown in **Figure 4.15** [40].

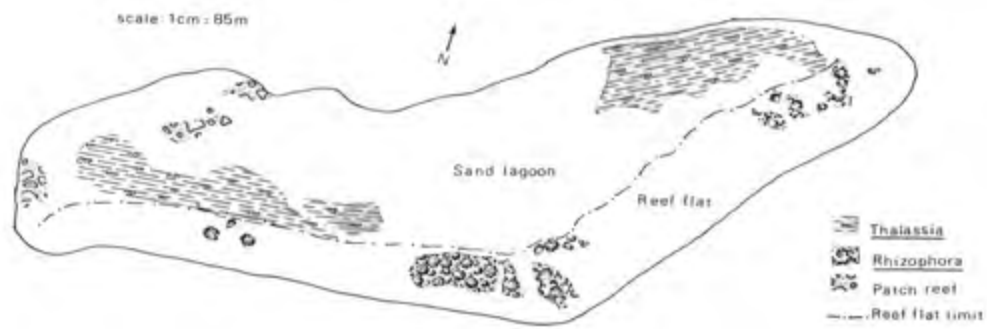


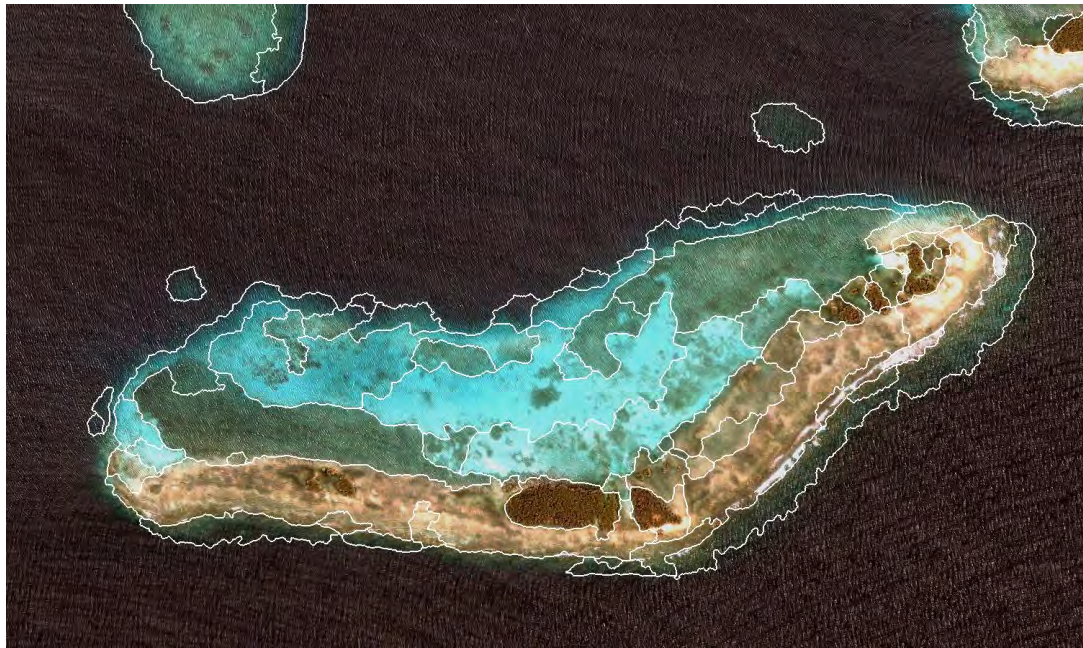
Figure 4.15 Classification map of Enrique Reef in 1980 [40]

The results of the segmentation algorithms using this image are given in **Figure 4.16**.

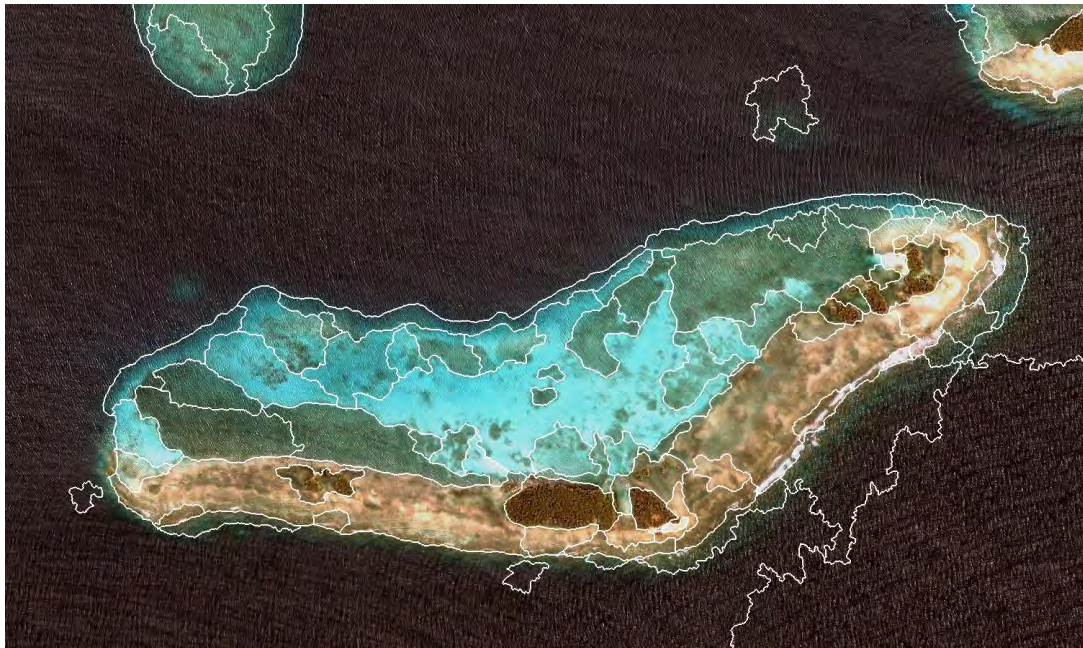


Figure 4.16 Segmentation results of Enrique Reef using local homogeneity analysis.





(a)



(b)

Figure 4.17 Segmentation results of **Enrique Reef** using: (a) Hurst coefficient / Hough transform and (b) perceptual image quantization.

The visual inspection for the evaluation of the segmentation of the algorithms is difficult due to the variability in shape, texture, and spectral response. Basically, all three algorithms performed very well in the identification of the homogeneous regions. Again, the coarsest segmentation is given by the local homogeneity analysis (**Figure 4.15**). This can be seen over the sand lagoon region where there is some mix of sand and *Thalassia*. Comparing visually the results of the Hurst coefficient/Hough transform (**Figure 4.16a**) and the perceptual image quantization (**Figure 4.16b**), the results achieved are similar. The HC/HT gives a more coarse segmentation in comparison with the perceptual image quantization but with better separation of the homogeneous regions. It is interesting that a part of the coral reef that is in deeper water in the southeast part of Enrique Reef is detected as a homogeneous region.

#### **4.4 Summary and discussion of results**

Analyzing the results it can be seen that between the algorithms some differences and problems arisen in the segmentation:

##### **1. Hough transform for boundary detection algorithm –**

The algorithm developed solves the problem of infinite line and the connectivity problem. Other challenges arisen like by the fact that the Hough transform is used for estimation of lines. Good segmentation results from objects like the pencil, the upper dead coral, and the lead weight, which are low varying shapes. Bad segmentation results if the objects of interest are very amorphous and circular objects. The edges of the amorphous and

circular objects do not add up in the Hough transform space analysis giving error in the line approximation.

## **2. Local homogeneity analysis algorithm –**

The algorithm gave the coarsest segmentation between the homogeneity based algorithms. The coarseness is due to the form the local homogeneity quantification is calculated and the region growing technique used. The homogeneity is computed and is used directly in the image, not like the other two homogeneity based algorithms. The algorithm starts the region growing from the seed minimums to the high values of the H-image. Many regions are merged together in the region growing because the high points dividing two regions are not so high and the region are merged. In the literature, this effect is called over spilling. Small regions with weak edges are merged together giving a coarse segmentation.

## **3. Hurst coefficient / Hough transform algorithm –**

In comparison with the perceptual image quantization algorithm, it gives a more coarse segmentation but with better separation of the homogeneous regions. The algorithm developed calculates the local homogeneity quantification with the Hurst coefficient using the Hough transform giving more accurate quantification of the local homogeneity. This method uses a multiscale quantification of the homogeneity and there is less impulsive noise because of the Hurst coefficient/ Hough transform quantification for homogeneity. Also, the same problem arises with the region growing

technique and the merging of small regions with weak edges giving a coarse segmentation.

#### **4. Perceptual image quantization algorithm –**

The algorithm gave the less coarse segmentation between the homogeneity based algorithms but the quantification of local homogeneity can not cope with impulsive noise in the local window, giving less separation of the homogeneous regions. A pixel in the local window can be impulse noise and be part of the peer group giving error in the clustering phase. Also, the same problem arises with the region growing technique and the merging of small regions with weak edges giving a coarse segmentation.

## **Chapter 5: Conclusion**

### **Preview**

This chapter consists of presenting a summary, achievements and conclusions concerning this thesis and recommendations for further work.

### **5.1 Summary**

The purpose of this work was to research and develop subsurface image segmentation algorithms that can be used for the monitoring and studying of coral reefs. One important tool in image processing that is investigated in CenSSIS is image segmentation. Image segmentation is an essential preliminary step for recognizing and analyzing coral reefs since it divide an image into parts that have a strong correlation with objects or areas of the real world contained in the image.

Since the images of interest are subsurface images, low contrast and noise is usually present. Segmentation algorithms for multispectral images generally are based on one of two basic concepts: contrast and homogeneity of the objects or regions contained in the image. An algorithm that takes in account the advantages of these two basic concepts is needed for the subsurface images. The following new algorithms were developed in this work: new Hough transform for boundary detection –clustering is used as a new modality to false contours elimination created by the Hough transform and Hurst coefficient using the

Hough transform –Hough transform and weighted c-means is used as a modality to calculate the Hurst coefficient and image spectral quantization. Two algorithms described in the literature were also studied: local homogeneity analysis, and peer image quantization.

## 5.2 Conclusions

The main purpose of CenSSIS is to study how to detect and create images of objects and conditions underground, underwater, or embedded within living tissue or manmade structures. Unfortunately, subsurface images are rich in both spectral variability and texture and are often noisy and contaminated. The algorithms researched and developed can cope in some extent with the characteristics of these types of images, each one having its advantages and disadvantages.

The new Hough transform for boundary detection is a powerful segmentation algorithm that can cope with noise and partially occluded or discontinued boundaries but it has some limitations. Some challenges of the Hough transform such as the end point problem and the connectivity problem are solved adding the clustering information of the image and eliminating those false contours. The limitation of the Hough transform is for image with extremely irregular and circular contours since the Hough transform is used for line estimation. For images where regular contours exist and there are not many objects, the algorithm work very well. Other versions of the Hough transform exist for shape analysis and recognition but the objects are needed *a priori*.



Since limitations with the new Hough transform for boundary detection exists, others algorithms based on homogeneity analysis were developed to solve the problem of image segmentation. The algorithms based on homogeneity analysis worked very well dividing the image in homogeneous regions. Note that the desired task of these algorithms is not the recognition of the objects, remember that the segmentation is a primarily task in the recognition and classification. The task is to divide the image in homogeneous regions that later can be studied and expanded for the recognition and classification.

The local homogeneity analysis algorithm gave the coarsest segmentation of the three homogeneity based algorithms. The only difference between this algorithm and the other two homogeneity based algorithms is that the part of clustering is not performed and the region growing is done directly in the image. The region growing and merging affect the details that can be seen in the final segmentation.

The Hurst coefficient using the Hough transform and peer image quantization had similar results. These algorithms performed a clustering before the region growing and merging techniques giving more region separation. The main difference between these two is that the peer image quantization gave the less coarse segmentation and less separation of homogeneity regions in comparison between the Hurst coefficient using the Hough transform.

The classification of the AUV images is a very difficult problem because of the variability in spectral signature of the corals from same species and the

background in the images. The classification using the Hurst coefficient using the Hough transform gave the best accuracy between the homogeneity based algorithms. Only four of the AUV images used in this work have a class map. The class maps for others AUV images are also needed for validating these techniques. Also, the remotely sensed images lack of more profound validity since a true newer class map for the IKONOS image cannot be found.

### **5.3 Future work**

More accurate validation for AUV and IKONOS images are required. A class map of the IKONOS image in La Parguera and more precisely Enrique Reef and class maps for other AUV images are needed. A quantification of the segmentation performance can be done with the class maps. Also, the algorithms can be performed on other subsurface images like biomedical and underground images to quantify its robustness in the CenSSIS diversity area.

One step that can be improved in the homogeneity analysis algorithms is the region growing and region merging techniques. The region merging algorithm only uses the centroid of the regions. A more reliable algorithm that can use the texture, spectral information, and the position relative to the other regions is needed.

## References

- [1] Francisco J. Rivera, Raúl E. Torres, and Luis O. Jiménez “Hough transform for robust segmentation of underwater multispectral images,” SPIE: AeroSense 2003-Technologies and Systems for Defense & Security, Orlando, 2003.
- [2] R. O. Duda and P. E. Hart, “Use of the Hough transform to detect lines and curves in pictures,” *Communication ACM*, vol. 15, pp. 11-15, 1972.
- [3] R. González and R. Woods, *Digital Image Processing*, 2nd ed. New Jersey: Prentice Hall, 2002.
- [4] John Richards and Xiuping Jia, *Remote Sensing Digital Image Analysis: An Introduction*, 3rd ed. New York: Springer-Verlag, 1999.
- [5] P.V.C. Hough, Method and Means for Recognizing Complex Patterns, *U.S. Patent 3069654* (1962)
- [6] M. C. K. Yang, Jong-Sen Lee, Cheng-Chang Lie, and Chung-Lin Huang, “Hough transform modified by line connectivity and line thickness,” *IEEE Transactions on Pattern Analysis and Machine Intelligence*, Vol. 19, Issue: 8 pp. 905-910, 1997.
- [7] N. Guil, J. Villalba, and E. Zapata, “A fast Hough transform for segment detection”, *IEEE Transactions on Image Processing*, vol. 4, no. 11, pp. 1541-1548, 1995.
- [8] M. Sonka, V. Hlavac, and R. Boyle, *Image Processing, Analysis, and Machine Vision*. PWS Publishing, 1998

- [9] L. da Fontura Costa and M. B. Sandler, "A binary Hough transform and its efficient implementation in a systolic array architecture," *Pattern Recognition Letters*, vol.10, pp. 329-334, 1989.
- [10] L. da Fontura Costa and M. B. Sandler, "The binary Hough transform-theory, real time implementation and application to visual inspection," *IEE Colloquium on Binary Image Processing - Techniques and Applications*, pp. 1/1 - 1/4, 1991.
- [11] L. Xu, E. Ojeda, and P. Kultaken, "A new curve detection method: Randomized Hough transform (RHT)," *Pattern Recognition Letters*, vol.11, pp. 331-338, 1990.
- [12] A.R. Hare and M.B. Sandler, "Improved-performance 'randomized' Hough transform," *Electronics Letters*, Vol. 28, Issue: 18 pp. 1678 -1680, 1992.
- [13] P. Fung, W. Lee, and I. King, "Randomized generalized Hough transform for 2-D gray scale object detection," *Proceedings of the 13th International Conference on Pattern Recognition*, Vol. 2, pp. 511 -515, 1996.
- [14] H. Li, M. A. Lavin, and R. J. Le Master, "Fast Hough transform: A hierarchy approach," *CVGIP*, vol. 36, pp. 139-161, 1986.
- [15] R. D. Duda and P. E. Hart, "Use of the Hough transform to detect lines and curves in pictures," *Communication ACM*, vol. 15, pp. 11-15, 1972.
- [16] R. K. K. Yip, "Line patterns Hough transform for line segment detection," *IEEE Transactions on Image Processing*, pp. 319-323, 1995.
- [17] T. Hanif and M.B. Sandler, "2D shape reconstruction from the Hough transform," *IEEE IEE Colloquium on Hough Transforms*, pp. 5/1 -P5/4, 1993.

- [18] J. Princen, K. Yuen, J. Illingworth, and J. Kittler, "A comparison of Hough transform methods," *Third International Conference on Image Processing and its Applications*, pp. 73 -77, 1989.
- [19] A. R. Hare and M. B. Sandier, "General Test Framework For Straight-line Detection By Hough Transforms," *IEEE International Symposium on Circuits and Systems*, pp. 239 -242, 1993.
- [20] J. E. Vuillemin, "Fast linear Hough transform," *Proceedings on the International Conference on Application Specific Array Processors*, pp. 1-9, 1994.
- [21] N. Aggarwal and W.C Kar, "Line detection in images through regularized Hough transform," *Proceedings of the 2000 International Conference on Image Processing*, Vol. 3, pp. 873 -876, 2000.
- [22] A. Tezmol, H. Sari-Sarraf, S. Mitra, R. Long, and A. Gururajan, "Customized Hough transform for robust segmentation of cervical vertebrae from X-ray images," *Proceedings. Fifth IEEE Southwest Symposium on Image Analysis and Interpretation*, pp. 224 -228, 2002.
- [23] Z. Yalin, M. S. Nixon, and R. Allen, "Automatic lumbar vertebrae segmentation in fluoroscopic images via optimized concurrent Hough transform," *Proceedings of the 23rd Annual International Conference of the IEEE EMBS*, Vol. 3, pp. 2653 -2656, 2001.
- [24] J. H. Han, L.T. Koczy, and T. Poston, "Fuzzy Hough transform," *Second IEEE International Conference on Fuzzy Systems*, Vol.2, pp. 803 -808, 1993.
- [25] Soodamani and Z. Q. Liu, "A novel fuzzy Hough transform for shape representation," *IEEE International Conference on Fuzzy Systems Proceedings*, Vol. 2, pp. 1605 -1608, 1998.

- [26] F. Jing, M. Li, H. Zhang, and B. Zhang, "Unsupervised image segmentation using local homogeneity analysis" Proc. IEEE International Symposium on Circuits and Systems, 2003
- [27] J. R. Parker, *Algorithms for Image Processing and Computer Vision*, 1st ed. New York: Wiley, 1997.
- [28] H. E. Hurst, R. Black, and Y. M. Simaika, *Long Term Storage: An Experimental Study*, London, Constable, 1965.
- [29] J. Feder, *Fractals*, 1st ed. New York: Plenum Press 1988.
- [30] J. C. Russ, "Processing with images with local Hurst operator to reveal texture differences," Journal of Computer Assist. Microsc., Vol. 2, pp. 249-257, 1990
- [31] J. C. Russ, *The Image Processing Handbook*, 3rd ed. Florida: CRC Press, 1999
- [32] Y. Deng, C. Kenney, M. Moore, and B. S. Manjumanath, "Peer group filtering and perceptual color image quantization," Proc. IEEE International Symposium on Circuits and Systems VLSI Vol. 4, pp. 21-24, 1999
- [33] F. J. Rivera, R. E. Torres, and L. O. Jiménez "Hough transform for robust
- [34] segmentation of underwater multispectral images," SPIE-The International Society for Optical Engineering Proceeding: AeroSense 2003-Technologies and Systems for Defense & Security, Orlando, 2003
- [35] J. C. Bezdek, *Pattern Recognition with Fuzzy Objective Function Algorithms*, 1st ed. New York: Plenum Press, 1981
- [36] J. C. Dunn, "A fuzzy relative of the ISODATA process and its use in detecting compact, well separated clusters," *Journal of Cybernetics*, vol. 3, pp.32-57, 1974

- [37] S. Araki, H. Nomura, and N. Wakami, "Segmentation of thermal images using the fuzzy c-means algorithm," *Second IEEE International conference on Fuzzy Systems*, Vol. 2, pp. 719-724, San Francisco, 1993
- [38] R. O. Duda and P. E. Hart, *Pattern classification and scene analysis*, 1st ed. New York: Wiley, 1973.
- [39] Y. Deng and B.S. Manjunath, "*Unsupervised segmentation of color-texture regions in images and video*" *IEEE Trans. on Pattern Anal. and Machine Intelligence*, Vol.23, No.8, pp. 800-810, Aug. 2001
- [40] R. Armstrong, "Changes in Cayo Enrique, La Parguera, Puerto Rico, from 1936 to 1980 using aerial photoanalysis" MS Thesis, University of Puerto Rico Mayaguez Campus, Department of Marine Science, 1981